Tectonophysics 846 (2023) 229664

Contents lists available at ScienceDirect

Tectonophysics

journal homepage: www.elsevier.com/locate/tecto

An updated view of the Italian seismicity from probabilistic location in 3D velocity models: The 1981–2018 Italian catalog of absolute earthquake locations (CLASS)

Diana Latorre *, Raffaele Di Stefano, Barbara Castello, Maddalena Michele, Lauro Chiaraluce

Istituto Nazionale di Geofisica e Vulcanologia, Rome, Italy

ARTICLE INFO

Keywords:
Earthquake catalog
Italian seismicity
3D probabilistic hypocenter location
Crustal seismogenic layer

ABSTRACT

We have built a complete catalog of three-dimensional (3D) hypocenter locations of earthquakes recorded in Italy from 1981 to 2018. Our catalog includes more than 420,000 events relocated by inverting a newly integrated dataset of ~5.0 million P and ~ 3.5 million S wave arrival times recorded by the Italian National Seismic Network and other permanent seismological networks operating in Italy. Available magnitudes are associated with earthquake locations from the most recent datasets and bulletins of Italian seismicity. Earthquakes are located in an updated 3D tomographic model of Italy obtained by including the Moho discontinuity and the seismic velocities of the Ionian subduction zone. We used a probabilistic, non-linear earthquake location code which provides complete information of the hypocenter solution uncertainties. Quality estimators of earthquake locations are analyzed a posteriori with an original criterion for a quantitative classification of the results, allowing users to select seismic events belonging to consistent quality classes and giving a more controlled image of the Italian instrumental seismicity for tectonic and geodynamical studies. The resulting catalog gives a new, coherent view of the spatial and temporal distribution of Italian seismicity. By selecting well constrained located events we construct the new Italian Crustal Seismogenic Layer (CSL) with a good spatial resolution, allowing us to show a comparison between seismogenic thicknesses and Moho geometry distribution. We finally present some examples of seismicity distribution in selected areas of Italy at regional and local scale relating the relocated events of our catalog with available multidisciplinary information from geology, geochemistry, geodynamical models, and historical seismicity.

1. Introduction

The Italian peninsula is a seismically active region that just in the last four decades was struck by six earthquakes with moment magnitude Mw $\geq$ 6.0 and several events with 5.5 $\leq$ Mw $\leq$ 6.0, all of these within seismic sequences lasting from several months to years (Rovida et al., 2020, 2022). The Istituto Nazionale di Geofisica e Vulcanologia (INGV) currently monitors Italy by managing the Italian National Seismic Network (hereafter RSN, Rete Sismica Nazionale) and other permanent networks in collaboration with Italian and European research institutions (Margheriti et al., 2021 and references therein). The Italian seismicity is located in real time by the surveillance system of the INGV and is afterward manually revised by the analysts of the Italian Seismic Bulletin (BSI) group that publishes an updated catalog of hypocenter locations and magnitudes every four months (http://terremoti.ingv.it/en/bsi, last accessed November 2022).

In the last years, several research projects focused on the construction of consistent catalogs of instrumental seismicity in Italy. The first catalog was the CSTI (Catalogo Strumentale dei Terremoti Italiani, CSTI working group, 2001, 2005), that provided standardized information of P and S phase arrival times, hypocenter locations, and magnitudes by merging seismic data collected from 1981 to 1996 by several permanent seismic networks. Later, an improvement of the CSTI catalog was compiled by Chiarabba et al. (2005) that extended the CSTI catalog of P and S phase arrival times including data recorded by seismic networks operating in Italy and surrounding regions for the period 1997–2002. Chiarabba et al. (2005) relocated the seismicity from 1981 to 2002 following a procedure based on an accurate tuning of location parameters and a new optimized one-dimensional (1D) velocity model of Italy. Thereafter, Castello et al. (2006) presented the CSI1.1 catalog (Catalogo

* Corresponding author.
E-mail address: diana.latorre@ingv.it (D. Latorre).

https://doi.org/10.1016/j.tecto.2022.229664
Received 22 April 2022; Received in revised form 31 October 2022; Accepted 20 November 2022
Available online 29 November 2022

della Sismicità Italiana, hereafter CSI) that updated the magnitude estimates of the relocated events from Chiarabba et al. (2005) by applying a regression analysis based on a relationship between ML and seismic coda duration. A further study was then focused on refining earthquake locations in a 1D velocity model of Italy using both a linearized inversion method and a parameter tuning similar to those previously applied for the CSI catalog (Chiarabba et al., 2015). This last study extended the computation of earthquake hypocenter locations up to 2012 by including the seismic phase arrival times of the Italian Seismic Bulletin.

All published catalogs of the Italian instrumental seismicity have the strength to cover long time periods, providing large and homogeneous datasets of hypocenter locations. Nevertheless, the hypocenter solutions presented in these catalogs suffer from varying levels of mislocation, often related to the focal depth determination because of the excessive simplification of the 1D velocity models used in the inversion procedure. In fact, velocity models did not account for effects of lateral heterogeneities that characterize the Italian velocity structure, to the detriment of the traveltime computation accuracy in the hypocenter location process.

In the last decade, a large amount of seismic data was made available by the INGV, thanks to the great improvement of the Italian National Seismic Network whose dense station coverage allows to detect small magnitude earthquakes (down to M_L 1.0) in most areas of the country (Schorlemmer et al., 2010). In the meantime, new studies provided accurate three-dimensional (3D) velocity models of Italy suitable for computing more reliable hypocenter locations (e.g., Di Stefano et al., 2009, 2011). In particular, Di Stefano and Ciaccio (2014) published a detailed tomographic model of Italy obtained by including the 3D geometry of the Moho discontinuity, previously constructed from both controlled source and teleseismic receiver function data. On the other hand, in the last twenty years, probabilistic, non-linear hypocenter location approaches have showed to be particularly efficient in relocating large amounts of data in complex 3D velocity models and has been successfully applied in many geological contexts at both local and regional scales (e.g., Lomax, 2005, 2008, 2020; Husen et al., 2003, Husen and Smith, 2004; Bethoux et al., 2016; Latorre et al., 2016, among many others). For these reasons, the updated catalog of Italian instrumental seismicity should include new data and make use of both 3D velocity models and efficient location methods to provide more accurate earthquake hypocenter solutions.

In this work we describe the catalog named CLASS (acronym for "Catalogo delle Localizzazioni ASSolute"), that is currently the most complete and homogeneous hypocenter location catalog of earthquakes recorded in Italy from 1981 to 2018. We have analyzed ~5.0 million P and ~ 3.5 million S wave arrival times, resulting from the largest collection of instrumental seismicity data recorded in Italy, in the wake of the CSI catalog by Chiarabba et al. (2005) and Castello et al. (2006), and enriched with new integrated seismic wave arrival times from both the INGV and other Italian permanent networks datasets. All the seismicity has been relocated in the 3D Italian tomographic model of Di Stefano and Ciaccio (2014) using the probabilistic, nonlinear earthquake location algorithm NonLinLoc (Lomax et al., 2000; hereafter NLL). Both the probabilistic approach and the nonlinear inversion method of NLL allow us to obtain a complete estimation of the hypocenter location uncertainties, whose parameters are then included in the innovative quality analysis proposed by Michele et al. (2019). This procedure provides a homogeneous, consistent catalog characterized by accurate 3D earthquake locations, robust evaluations of location uncertainties, and a quantitative "user friendly" classification of the results.

The CLASS catalog includes more than 420,000 earthquakes distributed along a time period covering the last four decades. By selecting well constrained located events, we construct the new Italian Crustal Seismogenic Layer (CSL) with a higher spatial resolution than previous versions, allowing us to propose a comparison between seismogenic thicknesses and Moho geometry distribution at regional scale. Through the analysis of our catalog we obtain a new general, coherent view of spatial and temporal distribution of the Italian instrumental seismicity. In particular, we present the seismicity of eight selected areas and we discuss some main characteristics enhanced by the analysis of the relocated events in light of available multidisciplinary information from geological and geochemical studies, geodynamical models, and historical seismicity data.

2. Seismotectonic context

The present tectonic setting in Italy (Fig. 1) is the result of many factors: 1) the larger scale evolution of the Mediterranean region after the closure of the Mesozoic Alpine Tethys (e.g., Dercourt et al., 1986; Dewey et al., 1989; Handy et al., 2010; Stampfli and Borel, 2002; Capitanio and Goes, 2006 among many others), 2) the collision between the Eurasia and Africa continents, 3) the curvature of the collisional zone between the African and Eurasian margins (Argand, 1924; D'Agostino et al., 2008), and 4) the subduction of the Mesozoic Ionian oceanic plate beneath the Tyrrenian lithosphere involving the slab roll-back and the opening of Neogenic back-arc basins (Faccenna et al., 2014). In particular, about 40 Ma ago, the continental lithospheres of the Adriatic and the European plates collided leading to the rise of the Alpine chain followed ~35 Ma ago by the construction of the Apennines chain. Then, 12–10 Ma to present, the slab retreat led to asymmetric opening of the Tyrrhenian Sea (Faccenna et al., 2004; Chiarabba et al., 2008; Di Stefano and Ciaccio, 2014).

The present geodynamical framework is well described by GPS velocities (D'Agostino et al., 2011). The Adriatic plate moves relative to Eurasia with increasing convergence rates across the Alps, from W to E, characterized by 2 mm/a of N-S shortening in the Eastern Alps (Grenerczy et al., 2005; D'Agostino et al., 2005) and extension along the Western Alps with right-lateral strike slip on NE-SW faults (Sue et al., 1999; Calais et al., 2002; Delacou et al., 2004; Thouvenot and Frechet, 2005; D'Agostino et al., 2008). Along the Apennines, increasing extension rates up to 3–4 mm/yr are measured from NW to SE while the Calabrian Arc, though still presenting extensional regime, shows peculiar behavior (D'Agostino et al., 2001; Hunstad et al., 2003). According to D'Agostino et al. (2011), this portion of the peninsula migrates southeastward relative to the subducting Ionian lithosphere with ~2 mm/yr of convergence absorbed in the Ionian wedge. The tectonic regime changes across the Messina Straits where crustal extension in Southern Sicily is clockwise rotated in the EW direction while part of the convergence between Europe and Africa is reflected offshore north of Sicily (D'Agostino and Selvaggi, 2004; D'Agostino et al., 2008; Montone and Mariucci, 2016).

Coherently with GPS velocities data, the seismicity of the Italian region is mainly characterized by extensional regime, especially along the Apennines where most of the last seismic sequences happened (Fig. 1). On the contrary, compressional regime is locally found: 1) offshore north of Sicily, 2) in the Eastern Alps at the outer front where the curvature from the Alpine belt to the Dinarides takes place, 3) along the Northern Apennines front and below the Po Plain, and 4) in the Adriatic Sea (D'Agostino et al., 2008; Montone and Mariucci, 2016; Magnoni et al., 2022). Most of the seismicity in Italy is mainly confined in the shallow crust, taking into account that about 90% of earthquakes are located above 20 km depth with some fluctuations in depth from Alps and Northern Apennines to Southern Apennines (Chiarabba et al., 2005; Chiarabba and De Gori, 2016). Sub-Moho seismicity is conversely present only where subduction is imaged by seismic tomography in the Northern Apennines and beneath the Calabrian Arc (Ciaccio et al., 1998; Lucente et al., 1999; Cimini and De Gori, 2001; Montuori et al., 2007; Chiarabba et al., 2008; Di Stefano and Ciaccio, 2014; Magnoni et al., 2022). In this latter region, the passive roll-back of the Ionian oceanic lithosphere still produces up to moderate magnitude earthquakes depicting a well-defined Benioff-zone down to 500 km depth (Chiarabba et al., 2015, and references therein).

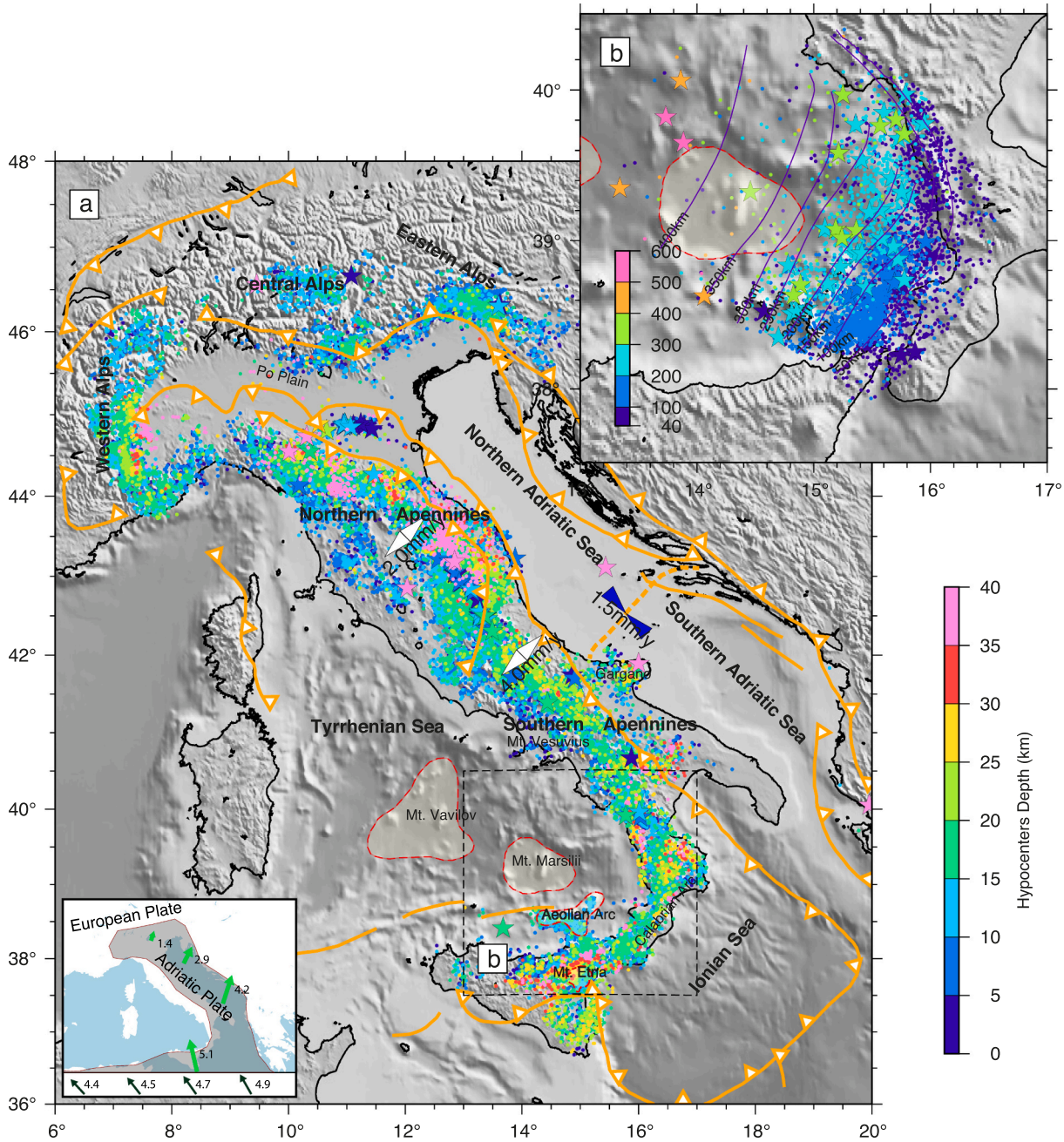

Fig. 1. Map of the Italian region with its principal geodynamic features (yellow lines) and instrumental seismicity relocated in the present work. a) Shallow earthquakes (0–40 km depth) selected for quality classes A and B (see section 3.3 for more details on the location quality). b) Deep earthquakes (40–600 km depth) of the Calabrian Subduction Zone, selected for quality classes from A to C. Red dashed lines delimit the main volcanic areas of the Southern Tyrrhenian Sea, Mt. Marsili, Mt. Vavilov, Aeolian Islands, and Mt. Etna. Depth isolines (purple lines) in (b) outline the top of the subducting Ionian lithosphere. Diverging (white) and converging (blue) arrows indicate the main orientations and rates of the deformation regime. Colour scale represents the hypocenter location depths in km. The inset is a simplified map (modified after D'Agostino et al., 2008) of the major plate boundary of the African/Adriatic plates (transparent gray) reporting, with light green arrows the representative velocities (in mm/yr) relative to Eurasia calculated from the GPS-derived poles of rotations; dark green arrows representa the velocities of North Africa relative to Eurasia. (For interpretation of the references to colour in this figure legend, the reader is referred to the web version of this article.)

Since 1981 the RSN of the INGV and other permanent regional networks have recorded about 420,000 earthquakes located in the Italian region and surrounding seas, 54 of them with magnitude M >5 (Fig. 1). Although the amount of events is strongly influenced by the progressively increased detection capability of our network, it clearly states the high rate of the Italian seismicity. The number of earthquakes is also variable year by year due to several seismic sequences. Beyond the Mw 6.5, 1976 Friuli earthquake (Eastern Alps, Rovida et al., 2020, 2022) and the Mw 6.9, 1980 Irpinia earthquake (Southern Apennines, Pondrelli et al., 2006) that are not included in the CLASS catalog, at least eight major seismic sequences following events with magnitude greater than 5.5 Mw struck Italy in the last 40 years (Table 1).

3. The 1981–2008 CLASS catalog

3.1. Integration of P and S wave arrival times and magnitude association

Italy and surrounding areas are currently monitored by more than

Table 1
List of the main seismic sequences recorded in Italy from 1981 to 2018 and included in the CLASS catalog (from Rovida et al., 2020, 2022).

Italian region	Year	Main Earthquakes
Monti della Meta (Central Italy)	1984	5.9 Mw and 5.5 Mw
Potenza (Southern Italy)	1990	5.8 Mw
Carlentini (Sicily)	1990	5.6 Mw
Colfiorito (Central Italy)	1997–1998	5.7 Mw and 6.0 Mw
Molise (Southern Italy)	2002	5.7 Mw and 5.7 Mw
L'Aquila (Central Italy)	2009	6.3 Mw and 5.5Mw
Emilia (Northern Italy)	2012	6.1 Mw and 5.9 Mw
Amatrice-Visso-Norcia (Central Italy)	2016–2018	6.2 Mw, 6.1 Mw, and 6.6 Mw

400 seismic stations belonging to the Italian seismic network managed by the INGV, whose signals converge to a centralized monitoring detection system (Margheriti et al., 2021 and references therein). In the past decades the station coverage of Italy was ensured by many different permanent networks such as the ING (currently INGV) and other institutions, seismic observatories, and University departments (Fig. S1, Supplementary Material). After 2005, the RSN strongly evolved due to the installation of new three component seismic instruments with an important improvement of the recorded signal quality.

To compensate for the relatively poor coverage of the RSN in the period 1981–1996, the CSTI working group (CSTI working group, 2001, 2005) integrated the data of the INGV seismic bulletin with P and S arrival time readings from other bulletins of regional permanent networks. Lately, Chiarabba et al. (2005) extended the data integration providing the 1981–2002 CSI catalog (Catalogo della Sismicità Italiana, Castello et al., 2006).

In the present work, we further extend the CSI catalog of seismic phases up to 2008 by applying the phases' integration method proposed by Chiarabba et al. (2005) and revising it by adding time-space post-processing controls on phase association based on both automatic and interactive inspection tools. In general, we observe that the new integration procedure strongly improves both catalog completeness and location quality because we increased the number of locatable events and the number of observations at stations close to the epicenters reducing the azimuthal gap.

For the last period of the catalog (2009–2018), P and S phase readings are extracted from the BSI catalog (the Italian Seismic Bulletin of the INGV; Nardi et al., 2020; Di Maro et al., 2022 and references therein; http://terremoti.ingv.it/en/bsi) since the detection capability of the RSN after 2009 became higher and wider on almost the whole Italian peninsula. Indeed, many of the non-INGV regional networks, whose phase readings were integrated in the CSI catalog, became part of the RSN database. P and S phase arrival times and signal amplitudes are first analyzed by the personnel on duty in the INGV Seismic Monitoring Room for civil protection purposes, and then revised by seismic analysts of the BSI working group for publication in the BSI bulletin.

The CLASS catalog of earthquake locations is obtained by inverting P and S wave arrival times from both the extended CSI catalog (1981–2008) and the BSI catalog (2009–2018). Event magnitude was not recomputed for our catalog, but obtained from previous available catalogs when this information is present. Magnitudes in CLASS (hereafter the "preferred Class magnitudes", Table S2.1 in the Supplementary Material) generally are local magnitudes (ML) whenever it is possible and within the range of the ML reliability. This is for the sake of homogeneity and completeness in a variety of studies. From 1981 to 2002, when the duration magnitude (Md) was the reference one of the INGV catalogs and the local magnitude (ML) was limited to few events (Mazza et al., 1998), the preferred CLASS magnitudes are inherited from the CSI catalog (Castello et al., 2007). For events without magnitude estimation in CSI, we have extracted this information from the ISIDe database (ISIDe Working Group, 2007) giving priority to the Md, INGV reference magnitude at that time (Table S2.1 in Supplementary Material). For events of the period 2003–2018, the preferred CLASS magnitudes are extracted from the ISIDe database, which also includes all the solutions from the BSI bulletin. In this case, ML when available represents the preferred CLASS magnitude. For further details about our choice of the preferred magnitudes in CLASS, the magnitude completeness in time and geographic distribution of maximum magnitudes, see section 2 of the Supplementary Material.

3.2. Hypocenter location method and parameterization strategy

We relocated the Italian seismicity with the hypocenter location program NLL (NonLinLoc, Lomax et al., 2000, 2014) which follows a probabilistic approach and uses a nonlinear inversion method. NLL provides a comprehensive estimate of the location uncertainties through the construction of the "a posteriori" probability density function (PDF) by solving the inversion problem formulation proposed by Tarantola and Valette (1982). Following this approach, the optimal earthquake hypocenter location is represented by the maximum likelihood point of the computed PDF, while both shape and size of the PDF characterize the hypocenter location uncertainty. NLL can manage hypocenter locations in very complex velocity structures since it uses both the 3D finite-difference (FD) code of Podvin and Lecomte (hereafter P&L code; Podvin and Lecomte, 1991) for traveltime computation to solve the forward problem, and the efficient oct-tree importance sampling algorithm to solve the inversion problem (Lomax and Curtis, 2001). Thanks to these characteristics, we were able to locate the CLASS events using the Italian 3D Tomographic Model proposed by Di Stefano and Ciaccio (2014). This is composed by a regularly spaced mesh with average vertical thickness of 15 km and seismic velocities linearly interpolated in 3D between grid nodes. The authors performed the tomographic inversion by introducing in the starting model a strong velocity contrast representing the 3D geometry of the Moho discontinuity to constrain Pn and Sn phases traveltimes following the Snell's Laws (Zhao et al., 1992, 1994).

In order to use the Italian 3D Tomographic Model for FD traveltime computation with the P&L code, we have resampled both P and S tomographic grids into finer grids of cubic cells with mesh spacing of 2 km and constant slowness inside each cell. The topography is not included in our parameterization, but the velocity model grid is extended up to the cells that include the seismic stations. By following the NLL procedure, P and S traveltime grids need to be computed for each seismic station and stored before solving the inversion problem. The main issue concerning earthquake locations at the Italian scale based on 3D, FD traveltime computation is the huge dimension of the traveltime grids involved in the inversion procedure, since the Italian seismicity is distributed in a target volume of about $1200 \times 1200 \times 800$ km^3 and recorded at more than 400 stations. Therefore, using cubic cells having 2 km $\times$ 2 km $\times$ 2 km size, we should manage hundreds of very large grids (up to $2{,}88 \times 10^8$ nodes for each station) making the hypocenter location of the entire catalog excessively time-consuming. To tackle this problem, we first calculate the traveltimes with the P&L code in the original finer grids of cubic cells with mesh spacing of 2 km to maintain precision, and then we decimate the computed traveltime grids for increasing depths by preserving the finer, 2 km-size grids in the upper crust (from the Earth's surface to 20 km depth) where we need a more detailed representation of the 3D structure, and doubling incrementally the cell size at specified depths, in the lower crust (4 km-size grid from 20 to 40 km depth), at lithospheric depths (8 km-size grid from 40 to 100 km depth), and in the upper mantle (16 km-size grid from 100 to 600 km depth). The conversion of the traveltime grids has been performed with the cascading grid module included in the NLL software (http://alomax.free.fr/nlloc). Using our parametrization, we estimated that typical errors due to the conversion from full regular grids to cascading grids are in a range of ± 0.1 s, lower than average picking errors estimated on P and S waves input data. On the contrary, resampled grids allow us to reduce by ~90% the size of each station-phase traveltime grid, making the earthquake location of the entire catalog

easier to manage.

Finally, in order to compensate for small-wavelength velocity heterogeneities not always sampled in 3D models at regional scale, we followed an inversion strategy including traveltime station corrections. We first perform a preliminary hypocenter location of the entire dataset, then we compute the mean value of traveltime residuals (i.e., the difference between observed and theoretical traveltimes) of well constrained event locations at each seismic station. These mean traveltime residuals represent the station corrections that are later added to the theoretical traveltimes in the final computation of hypocenter locations.

3.3. Quality assessment and classification of location results

The validity of a hypocenter location is generally assessed "a posteriori" by analyzing the inversion solution uncertainty that is defined by many kinds of estimators related to the picking quality, the earthquake-station geometry and inversion method/approach. Michele et al. (2019) showed that all the uncertainty estimators of a hypocenter location are linked to each other and can be combined in a unique empirical formula. Following this formula, we assess the quality of the CLASS catalog using seven main location estimators that are reported in Table 2 and Figure S3 of the Supplementary Material.

For each event, hypocenter location estimators of Table 2 are first normalized to take into account their different physical units, then they are combined in the empirical formula providing a unique location quality factor. Since we deal with a catalog that spans a time period of 40 years, we need to consider that input and output data qualities are not always homogeneous due to the change of the acquisition system and the variability of the seismic activity over time. For this reason, data normalization has been performed with respect to the 90th percentile of each kind of location estimator allowing us to reduce the influence of possible outliers and providing a more stable and homogeneous classification of our results. Finally, in order to set up a simple way for selecting events in our catalog, we associated each location quality factor to a quality class having code from A (best location with quality factor from 0 to 0.25) to D (worst location with quality factor from 0.75 to 1).

Maps in Fig. 2 show the distribution of the earthquakes divided by the quality class they belong to (A-class, B-class, C-class, and D-class). Inset in Fig. 2a indicates that event location quality is excellent for some 24% of the catalog (~101,900 events, A-class), good for 42% (~178,500 events, B-class), poor for 21% (~87,600 events, C-class), and bad for 13% (~54,500 events, D-class). A-class seismicity (Fig. 2a) is mainly concentrated along the Apennines chain, especially in its northern sector where main seismic sequences occurred in the last 40 years (Table 1) and where the station coverage was able to provide very good quality hypocenter locations (see Fig. S1 in supplementary material). A-class seismicity is also present in Northern Italy, both in the Western and the Eastern Alps, and in a very small area of the Po Plain where temporary seismic stations were installed during the 2012 Emilia sequence in addition to the RSN. B-class seismicity (Fig. 2b) is distributed all along the Alps, the Apennines, the Calabrian arc and in Sicily. B-class is the most representative quality group of the catalog: it is mainly concentrated on land where we have a good acquisition geometry, but also offshore, North of Sicily, where the seismic stations installed in the Aeolian Islands reduce the azimuthal gap of the source-station geometry. C-class (Fig. 2c) shows a distribution quite similar to the B-class, although more scattered: it concerns hypocenter locations with high values of uncertainty estimators, also including deeper events along the Ionian subduction zone that have large azimuthal gap values due to the RSN coverage. D-class seismicity distribution (Fig. 2d) presents a very scattered image with earthquakes completely covering Italy and surrounding seas although this class only includes some 14% of the catalog. Hypocenter locations of D-class are obtained by inverting poor quality data, with very few seismic phases and/or recorded at very sparse station networks. Generally events located offshore like the clusters in the Adriatic and Tyrrhenian Sea, or inland like those at the edge of our network belong to D-class.

In the next sections, we will refer to the best quality event locations (i.e., both A-class and B.-class events), which correspond to the 66% of the catalog (about 280 k events) and well represent the Italian seismicity distribution. However, we also include the C-class hypocenter locations to better discuss the offshore seismicity in the Tyrrhenian sea along the subduction zone of the Calabrian arc since this region mainly includes this latter quality class due to the peculiar network coverage.

Table 2
List of estimators of the hypocenter solution uncertainty used in the present work to compute the quality factor of a location as defined in the empirical formula from Michele et al. (2019).

Estimator	Description
rms	root mean square error from P and S arrival time residuals
nphs	number of arrival time picks used in the hypocenter location inversion
sdist	minimum station epicentral distance
errh	hypocentral error on horizontal coordinates computed from the 68% ellipsoid error
errz	hypocentral error on vertical coordinates computed from the 68% ellipsoid error
gap	maximum azimuthal angle between two successive stations around the source epicenter
Rpdf	radius of a sphere having volume equivalent to the PDF volume

4. The new map of the Crustal Seismogenic Layer

The Crustal Seismogenic Layer (CSL hereinafter) is the range of crustal depths in which most earthquakes happen (Scholz, 2019 and references therein). Lateral variation of its thickness gives important hints about the seismic hazard that is related to the maximum earthquake nucleation depth and the potential vertical extent of the faults. The base of the CSL roughly corresponds to the brittle-ductile transition zone; it depends on the composition and physical state of the rocks, and is strongly influenced by the geodynamics of the investigated zones (Watts and Burov, 2003; Scholz, 2019).

Depth location robustness in an earthquake catalog is crucial to correctly define the CSL vertical extent. Chiarabba et al. (2005) produced a first map of the CSL in Italy, based on 1D earthquake locations of the CSI catalog selected above 25 km depth. Afterwards, Chiarabba and De Gori (2016) refined the CSL map with relocated earthquakes from 2005 to 2015 extracted from the BSI catalog (ISIDe Working Group, 2007). The authors selected events above 30 km depth with a simple criterion based on both rms and vertical error estimators (Table 2).

In the present work we propose an updated version of the Italian CSL, based on the CLASS catalog, reporting the depth extent of the seismogenic layer with respect to the sea level. The lateral variation of this value is obtained by dividing the Italian peninsula in cells of ~20 km × 20 km having 75% of overlap in both latitude and longitude. This shift leads to a 5 km side final pseudo-grid. The contributing earthquakes are selected by the quality factor, including both A- and B-classes representing 66% of the catalog (~280,000 events). These classes ensure us to select strongly constrained events having also low formal vertical errors (82% ≤ 4 km, 50% ≤ 2 km). Using the quality factor in place of the only formal vertical error ensures us to reject almost all those unconstrained events with small vertical errors only due to model overfitting (Michele et al., 2019). To estimate the representative percentage of earthquakes defining the base of the CSL (i.e., the seismicity depth cut-off) we investigate the depth distribution quantiles, from 5% to 100%. The tradeoff choice resulted in 90% in agreement with Chiarabba and De Gori (2016).

Our updated CSL map shows an improved resolution with respect to the previous ones, due to two key aspects. First, we selected a much larger dataset: the number of high quality CLASS events for the CSL construction is twice that used in previous CSL maps. This noticeable

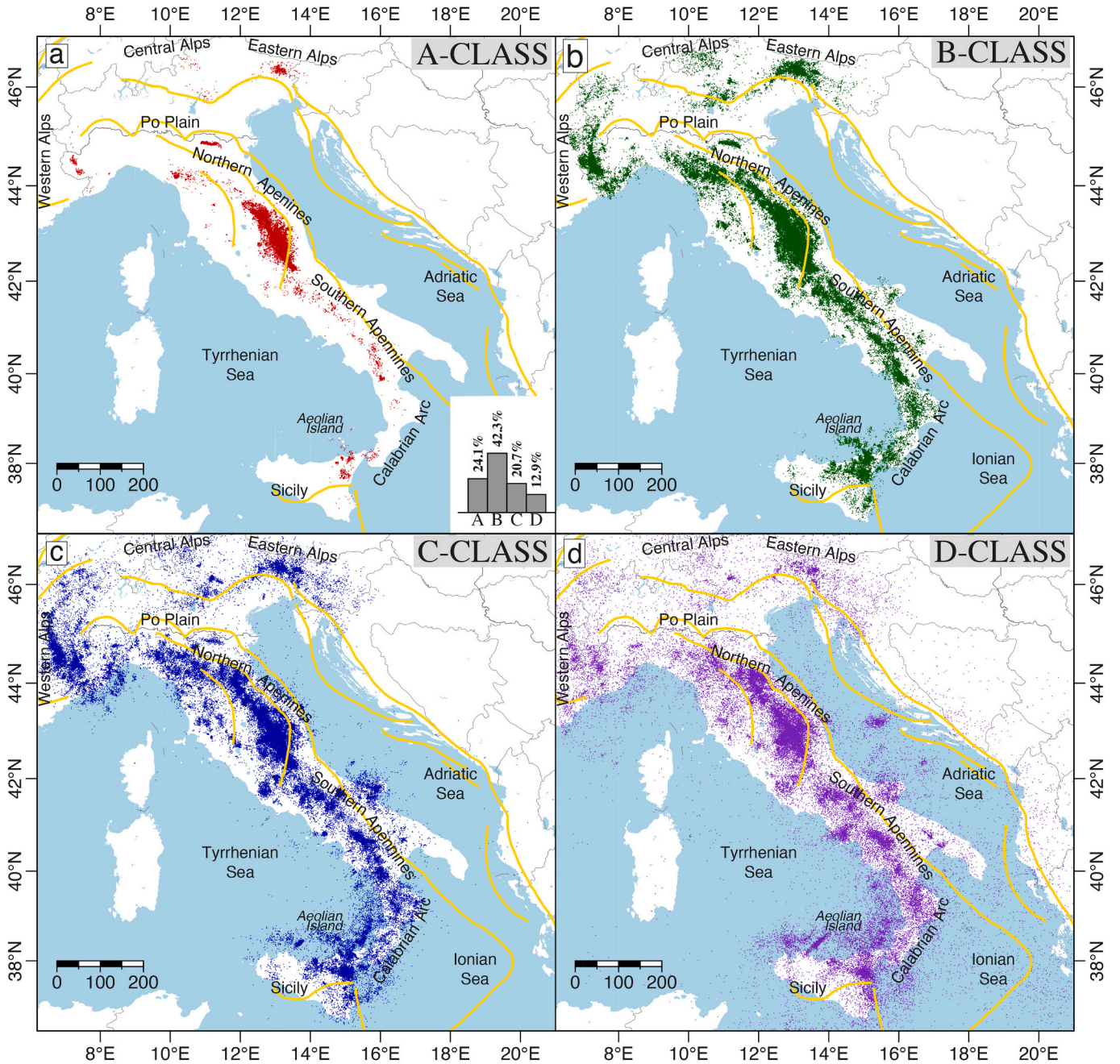

Fig. 2. Map view of the Italian seismicity recorded from 1981 to 2018 and relocated for the CLASS catalog. Each panel represents events belonging to a given location quality class (see text): A-class (red symbols, panel a), B-class (green symbols, panel b), C-class (blue symbols, panel c), and D-class (purple symbols, panel d). Inset in Fig. 2a shows the percentage distribution of the different quality classes of the catalog. Yellow lines represent the main tectonic alignments reported in Fig. 1. (For interpretation of the references to colour in this figure legend, the reader is referred to the web version of this article.)

increase of data allows us to keep the cells as small as 20 km × 20 km with great reduction compared to the 80 km × 80 km cell size of Chiarabba and De Gori (2016). Second, to account for the extremely variable thickness of the crust in Italy, related to the complex interaction and the different nature of the Adriatic, Tyrrhenian, and European tectonic plates, we select the crustal earthquakes by using the Italian Moho map (Di Stefano et al., 2011) avoiding the introduction of any flat arbitrary depth. Finally, we compute the error in the CSL depth estimation, in terms of standard deviation, with the bootstrap procedure over all the cells with the quantile 90 and 1000 iterations (Efron, 1979; Chiarabba and De Gori, 2016). Further details about the trade-off percentile and the bootstrap analysis are available in section 4 of the Supplementary Material. We produce the CSL map only plotting well constrained values obtained in cells sampled by at least 20 events.

The new Italian CSL map reported in Fig. 3a shows regional scale (low-frequency) and local scale high frequency upwards (blue tones) and downward (red tones) variations around a general predominance of the 13–18 km depth range (see the inset in Fig. 3a).

Most of the local scale, high frequency variations (spots) of the new CSL were not evidenced in the previous map by Chiarabba and De Gori (2016) while they are now well identified thanks to the improved resolution and the reduced horizontal smoothing of the image. For example, the wide area of high depths reported under Sicily and Calabria in Chiarabba and De Gori (2016), is now splitted into two parts, separated by a shallow depth area of the CSL along the Messinian strait extending toward the Aeolian Arc. Also, the relatively shallow depth

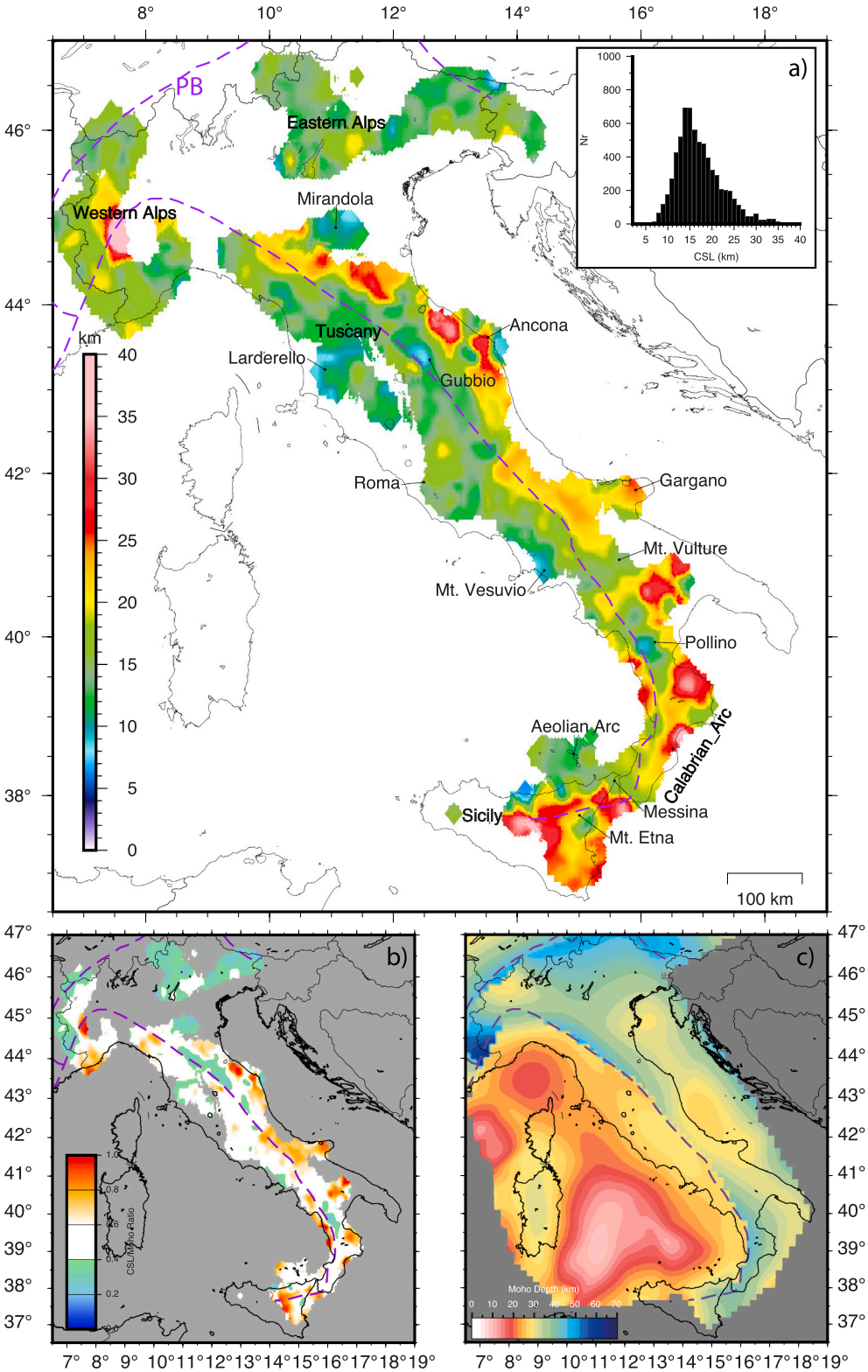

Fig. 3. a) Map view of the Crustal Seismogenic Layer (CSL) computed using the relocated events of the CLASS catalog. Colours represent the CSL depth; the map of the CSL resolution (σ in km) computed with the bootstrap method is available in the Supplementary Material (Fig. S4.1); the inset reports the distribution of the CSL depth values over the whole region; b) map view of the CSL/Moho depth (CM) ratio, an a-dimensional parameter calculated over each 5 km spaced pseudo-grid cell as the ratio between the depth of the CSL and the corresponding depth of the Moho under the same cell; c) map view of the Moho depth in the Italian region modified after Di Stefano et al. (2011); the dashed purple line is the plate boundary at moho depth (PB). (For interpretation of the references to colour in this figure legend, the reader is referred to the web version of this article.)

beneath Mount Etna volcano (Sicily) is well isolated in our image. This shallow depth feature, likely directly related to the volcano activity, is located within a regional scale area of high CSL depths corresponding to the deepening Ionian Moho.

There are several areas showing high frequency spots of CSL depth (e.g. Mt. Pollino, Mt. Vesuvius, the Mirandola structural high, Gubbio). Nevertheless the interpretation of these local variations would claim for a specific and focused analysis that takes into account many different local factors (e.g. composition and physical state of the rocks, presence of fluids, magmatism) that can interact with the large scale factors (e.g. the crustal thickness or the type and maturity of the lithosphere). For these reasons, this kind of analysis is beyond the scope of the present work.

A first sight to the large-scale features of our CSL map highlights that

upward and downward variations are not equally distributed over the Italian region. In Figs. 3a-c we report the plate boundary (PB, dashed purple line) at the Moho depth, from Di Stefano et al. (2011), highlighting the contact between the European, Adriatic and Tyrrhenian lithospheres. The final image helps to point out that the highest CSL depths are found in the eastern and southern side of this limit, within the Adriatic/Ionian plate where the lithosphere is highly flexed, pulling down the fragile portion of the crust. By comparing the CSL map (Fig. 3a) with the Moho map (Fig. 3c) the position of the high CSL depth areas seems to follow the Adriatic Moho depth isolines of 30–35 km. Moreover, the red areas of the CSL seem to easen where the Adriatic Moho is flatter (between Ancona and the Gargano promontory). This large scale dependency of the CSL upon the Moho depth might explain why almost all the Tyrrhenian side of the CSL map shows shallower depths than the Adriatic side, beyond the local thermal effect of the asthenosphere under the Tuscany magmatic province (Chiarabba and De Gori, 2016).

To further investigate this aspect, in Fig. 3b we report the ratio between the CSL and the mean Moho depths computed in each cell (hereafter called CM ratio). This parameter might help to normalize the CSL depths in regions characterized by very different crustal thickness, highlighting at the same time the stronger anomalies. This empirical analysis seems to show that most of the Italian region is characterized by a CM ratio of 0.4–0.6 (white colour), meaning that about half of the crust is generally characterized by fragile behavior. However, the variation around this range is not equally distributed in the region. For example, in the Eastern Alps the CSL is extremely shallow (CM < 0.4) over a wide area despite the high thickness of the crust (Fig. 3c). In the Northern Apennines, a narrow NW-SE oriented band with CM ≤ 0.4 is present immediately to the NE of the PB. The comparison with the Moho map (Fig. 3c) indicates that here the CSL is essentially related to the upper Adriatic crust that is involved in the belt deformation and decoupled from the downward flexed lower crust and Moho, probably due to the crustal delamination process suggested by several authors (Serri et al., 1993; Chiarabba et al., 2015; D'Acquisto et al., 2020). Another relevant anomaly of the CM ratio is located in the Southern Apennines between the PB and the Gargano promontory. Here we find a wide area where up to 80% (orange to red tones) of the thick Adriatic crust is involved in fragile deformation. This evidence is probably related to the peculiar seismotectonics of this area, where several models suggests the presence of pre-existing W–E trending deep strike–slip seismogenic sources, accommodating the Adriatic intraplate deformation inducing moderate-to-strong deep earthquakes (see Fracassi et al., 2004; Valensise et al., 2004; Latorre et al., 2010; Trionfera et al., 2020; Ciaccio et al., 2021 among many others).

In the next section, the new CSL will be presented in the figures of vertical cross sections as a term of comparison with the seismicity distribution.

5. Discussion on the relocated seismicity at regional and local scale

In the following sections we present and discuss some images of the seismicity distribution in eight selected areas where our catalog provides some new elements that might contribute to a better understanding of the Italian tectonic context. In each area the seismicity shows different peculiar characteristics; for this reason we propose different scale views (from regional to local) and a comparison with different kinds of data from literature (structural maps, geological sections, geochemical models, and historical seismicity) depending on the main information that the hypocenter locations of our catalog can provide. In particular, the selected areas (Fig. 4) cover: 1) the Alpine mountain chain (northern Italy) for which we overlay the relocated seismicity to available structural maps and geological vertical sections of its western and central-eastern parts (sections 5.1 and 5.2, respectively); 2) the Tuscan-Emilian sector of the Northern Apennines (section 5.3) where we analyze the seismicity in the light of geochemical models of deep source origin for CO2 fluxes (Chiodini et al., 2004), and where in 2012 the RSN recorded a seismic sequence that followed two main events of magnitude Mw 6.1 and Mw 5.9 (Table 1); 3) the Umbria-Marche sectors of the Northern Apennines (section 5.4) with a focus on the major seismic sequences of the last twenty years (Table 1) and their comparison with the continuous background seismicity; 4) the Northern-Southern Apennines transition zone (section 5.5), where M 6–7 earthquakes occurred in pre-instrumental times, up to 1915, followed by a long lasting seismicity "gap"; 5) the Southern Apennines (section 5.6) with a focus on the area where the Mw 6.9 Irpinia earthquake occurred in 1980 and 6) the Calabrian arc (section 5.7) where the relocated seismicity provide a detailed image of the subducted Ionian lithosphere.

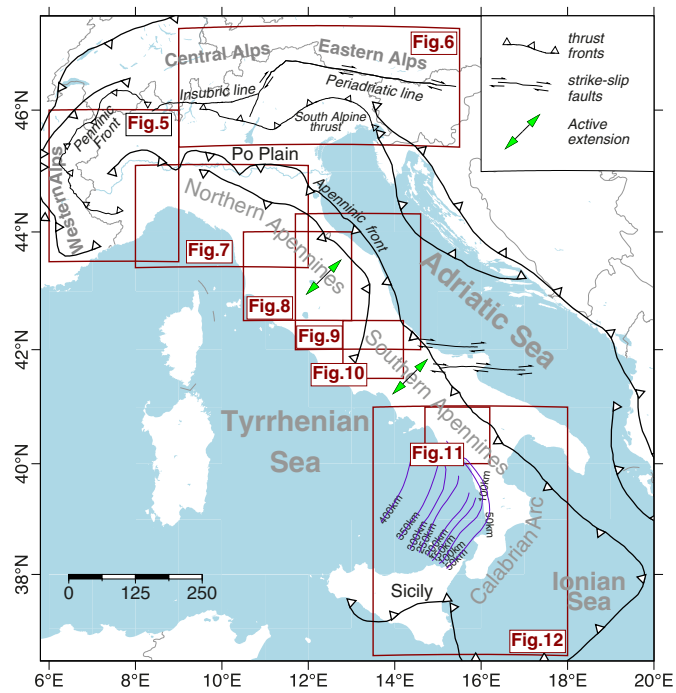

Fig. 4. Simplified sketch with the main tectonic features of Italy. Red boxes are the eight areas selected to present the CLASS catalog of earthquake locations. References related to the main features shown in this sketch are reported in detail in each area description. (For interpretation of the references to colour in this figure legend, the reader is referred to the web version of this article.)

5.1. Western Alps

In the Western Alps, the seismicity is essentially concentrated into two main branches that follow the Alpine belt curvature and converge toward the Ligurian Sea to the south (Fig. 5a). This distribution is in agreement with the work of Eva et al. (2020) showing a detailed comparison between instrumental seismicity and local main tectonic features. Here, we compare our results with the structural map of the Western Alps by Bousquet et al. (2012) in Fig. 5a, and with two geological vertical profiles called Argentera (Fig. 5b) and Pelvoux (Fig. 5c) by Schmid et al. (2017).

A first order observation is that the seismicity is roughly confined above 20 km depth with a slightly shallower seismogenic depth west of the Penninic Front and a deeper cluster at about 40 km depth to the east (at a distance of ~150 km along Fig. 5b), in agreement with Eva et al. (2015) and Malusà et al. (2017). Both vertical cross sections show that the geometry of the two seismicity branches observed in the map is driven at depth by the tectonic contact between internal and external Western Alps, namely the Penninic Front. Along the Argentera profile (Fig. 5b), the two clusters are very close to this tectonic contact, with a

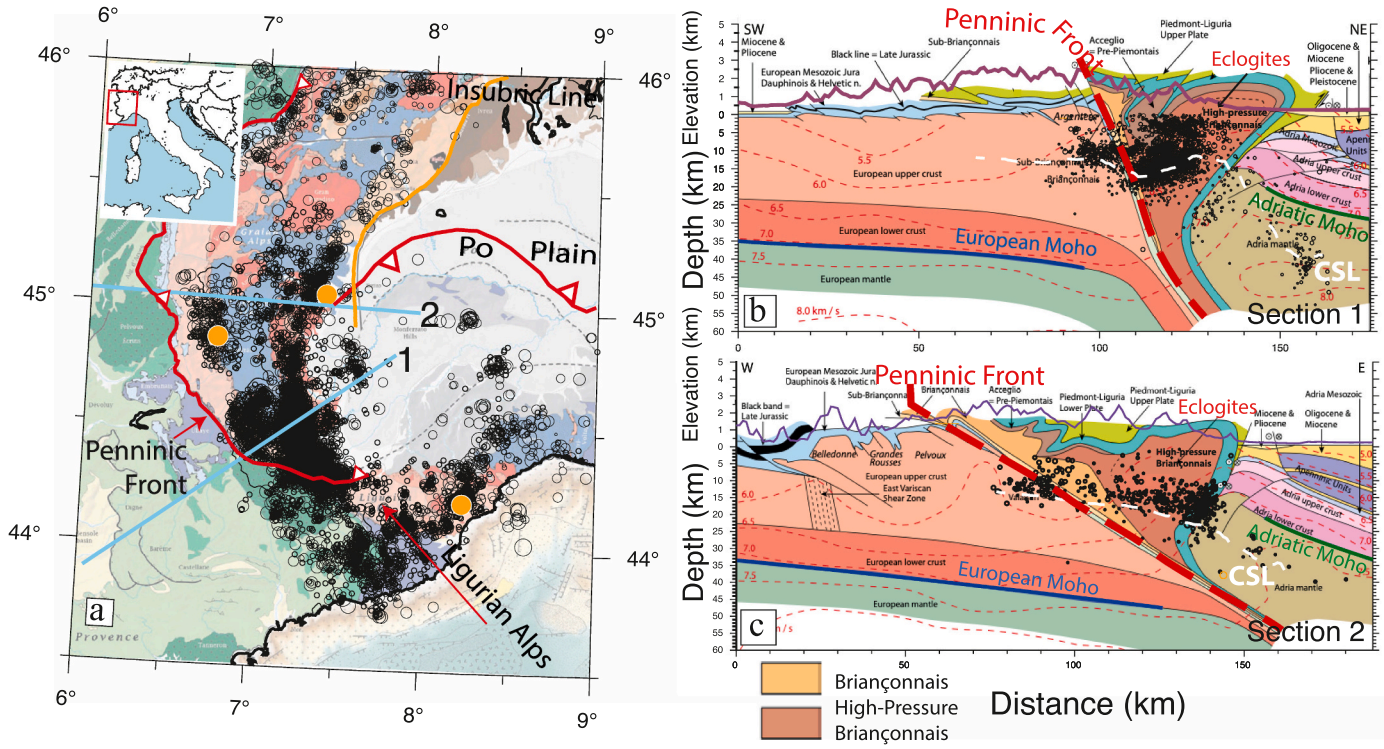

Fig. 5. a) Map of the seismicity distribution in the Western Alps overlaying the tectonic map proposed by Bousquet et al. (2012): black open circles are M < 4.0 earthquakes, orange solid circles are 4 ≤ M ≤ 5.0 earthquakes, skyblue solid line are the traces of the vertical sections reported in b and c; b) vertical section 1 cut along the Argentera profile (Schmid et al., 2017); c) vertical section 2 along the Pelvoux profile (Schmid et al., 2017); black dots in both sections are the hypocenters, the white dashed line represents the CSL depth, the purple solid line is the topographic local profile, the red thick dashed line and the red thin dashed lines are the Penninic tectonic front and the P-wave velocity isolines respectively as from Bousquet et al. (2012). (For interpretation of the references to colour in this figure legend, the reader is referred to the web version of this article.)

rough 5 km throw. In particular, to the west of the Penninic Front, the seismicity is located into the European upper crust, while to the east the hosting rock units appear to be the High-pressure Briançonnais eclogites (Schmid et al., 2017). This evidence is confirmed in Fig. 5c, where the two clusters belonging to the two seismicity branches, are separated by a region of sparser seismicity that roughly corresponds to the presence of the Briançonnese unit. In both vertical profiles we observe that the intense seismicity stops toward east since the Adria crustal volume does not show significant earthquakes, while very rare and sparse seismicity is located in the Adria mantle. This rapid change in the seismicity rate is better evidenced along the Pelvoux profile (Fig. 5c) at the tectonic contact between the High-pressure Brianconnais formation to the west and the Adria lithosphere to the east, showing a remarkable match between the relocated seismicity of the CLASS catalog and the geological models of this region.

5.2. Central and Eastern Alps

Map view of the Central and Eastern Alps seismicity (Fig. 6a) is imaged over the tectonic scheme proposed by Bousquet et al. (2012) while the three vertical cross sections (Figs. 6b-6d) are chosen taking into account information from literature on major tectonic lines and fault systems.

The first order features of the earthquake distribution highlight a general clustering along the maximum curvature of the main tectonic lines, namely the South Alpine Thrust to the east (red line in Fig. 6a) and the Insubric Line/Periadriatic Line to the west (Tonale and Pusteria Faults, orange lines) that marks the tectonic contact between the Northern and the Southern Alps. Clusters are also found north of the Insubric Line and close to the South Alpine Thrust. Conversely, the seismicity appears quite absent across Mt. Adamello area (red area in Fig. 6a) where a huge intrusive magmatic body is present (Callegari and Brack, 2002).

The seismicity of the South Alpine area is mostly concentrated along the Giudicarie SW-NE fault system (section 1, Fig. 6b). This seismicity is shown in section 2 (Fig. 6c) in closer detail. North of the Giudicarie Faults System, several M > 4 events occurred up to the Mw 4.8 earthquake of 2004-11-24 (orange symbols). Here, the seismicity that extends in the crust down to 15–20 km depth, is mainly concentrated in the western part of the profile, beneath the Giudicarie fault system while it is more sparse toward the east in correspondence with the N-verging Adriatic front of the Alps.

In section 3 (Fig. 6d), we focus on the seismicity distribution with respect to the South Alpine front, in a zone of compressive regime where a Mw 6.5 earthquake struck the area in 1976 (Rovida et al., 2020, 2022). By comparing our results to published tectonic reconstructions (Grad et al., 2009; Bousquet et al., 2012) we observe that the hypocenter distribution is very dense and almost confined in the Adriatic crust, down to 15 km depth, and beneath the tectonic contact between the Southern Alps and the External Dinarides. A volume of sparse seismicity separates this large cluster from that related to the seismicity around Bovec (Slovenia) where two M > 5.0 events occurred on 1998-04-12 and 2004-07-12.

5.3. Northern Apennines: The Tuscan-Emilian sector

The transition from the Alps to the Apennines chain is located between the southernmost part of the Western Alps and the northernmost part of the Northern Apennines, north-east of the Ligurian Sea (Figs. 1 and 7a). By considering the seismicity recorded in the last 40 years, this transition around the Sestri-Voltaggio Zone (SVZ, red polygon close to Genova in Fig. 7a) shows very sparse, low magnitude seismicity, at least

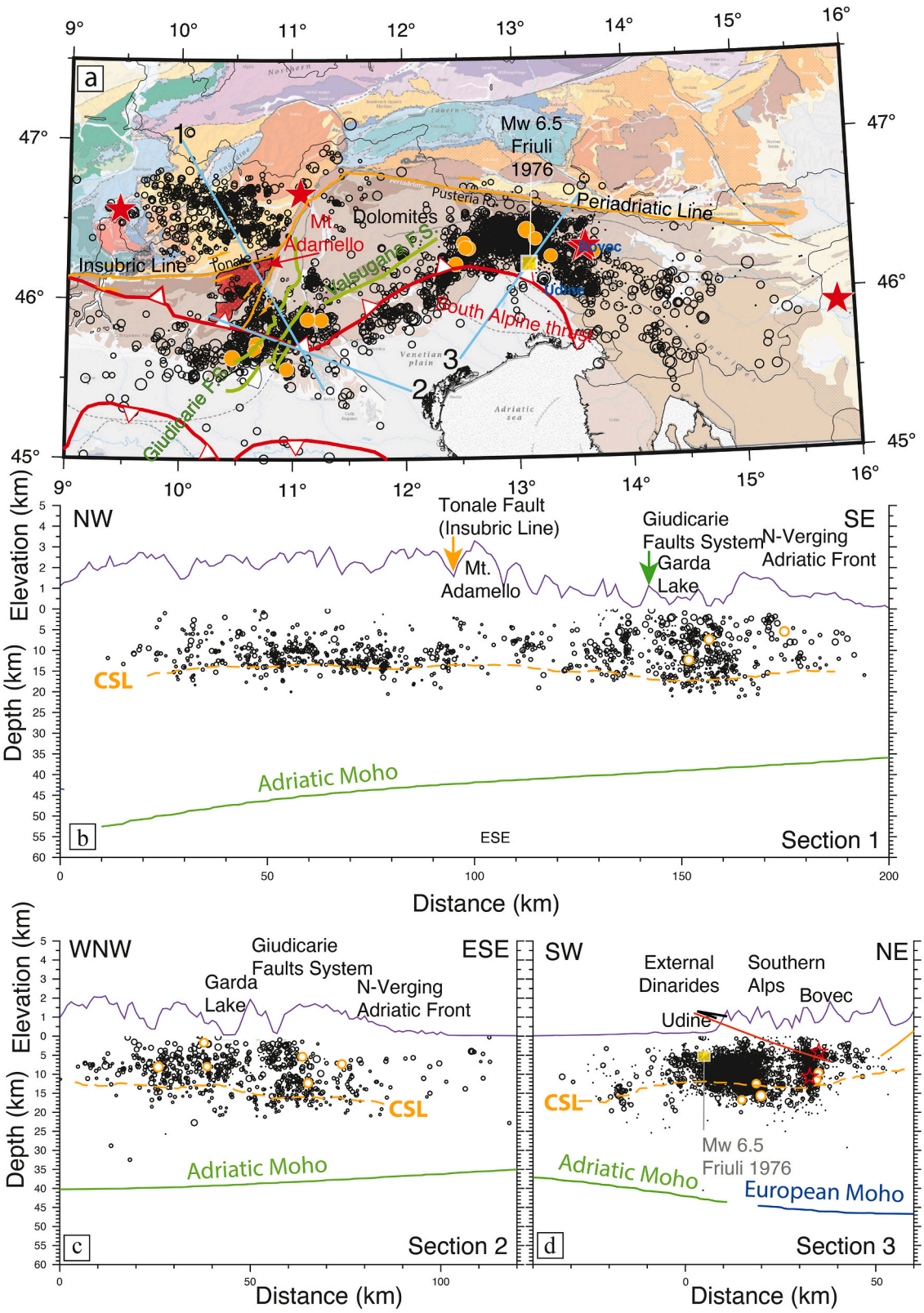

Fig. 6. Seismicity distribution in the Central and Eastern Alps. a) Epicentral distribution overlayed to the "Tectonic Framework of the Alps" (Bousquet et al., 2012). Sky-blue solid lines are the traces of the vertical sections 1–3, open black circles are earthquakes with M < 4.0; orange circles are 4 ≤ M < 5 earthquakes (open in the vertical sections and solid in the map), red stars are M ≥ 5 earthquakes (open in the vertical sections and solid in the map), black dots are earthquakes with no magnitude attributed; the Mw 6.5 Friuli 1976 hypocenter (yellow square in map and vertical section 3) is by Slejko et al. (1999); the orange dashed line in the vertical sections represents the CSL depth (Fig. 3); the solid red line and orange line in vertical section 3 are the Southern-Alpine Thrust and the Periadriatic Line respectively; the solid green line is the Adriatic Moho and the blue solid line is the European Moho. (For interpretation of the references to colour in this figure legend, the reader is referred to the web version of this article.)

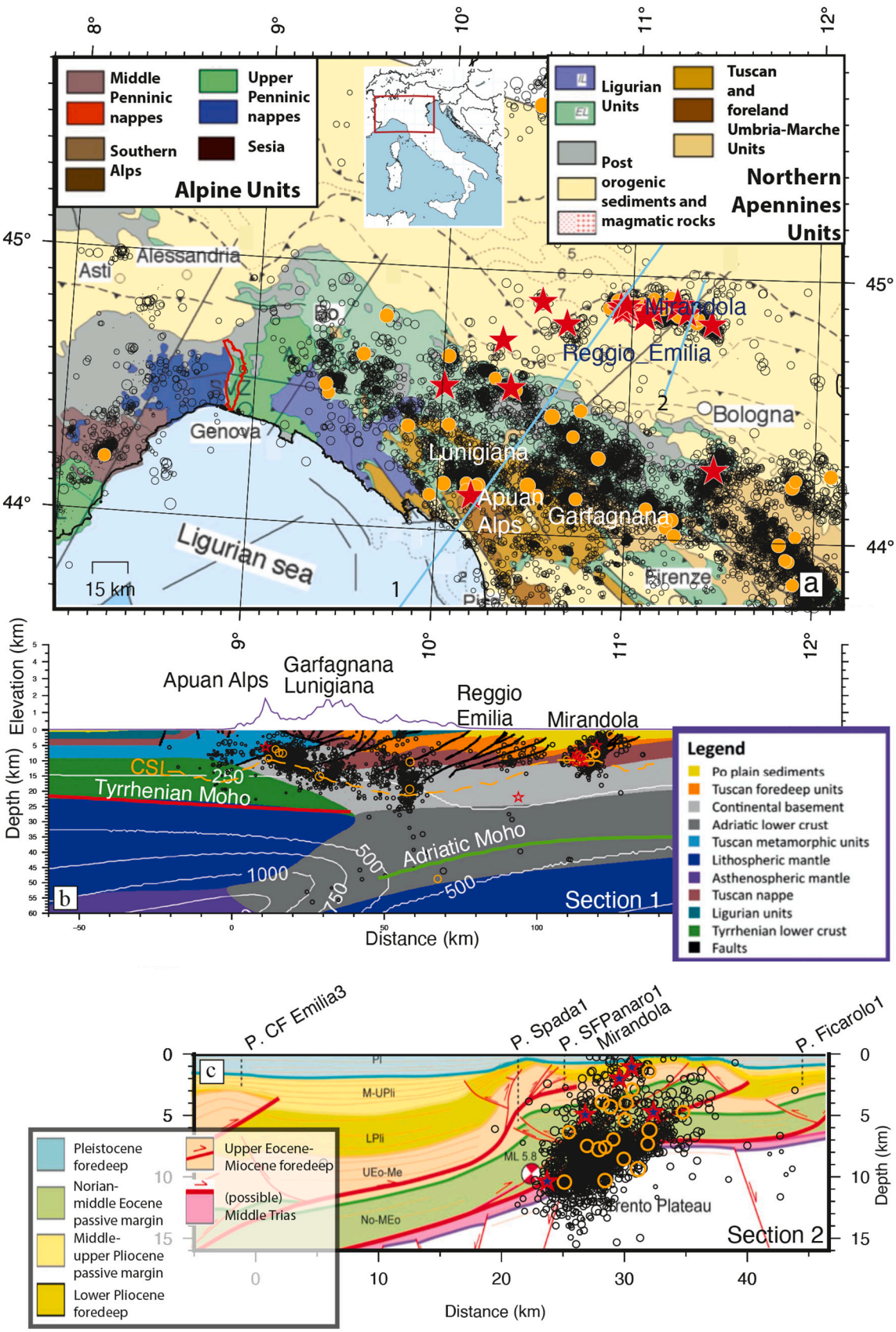

(caption on next page)

Fig. 7. a) Map view of the seismicity distribution presented over a geological and structural map from Molli et al., 2010; the red empty polygon close to Genova is the Sestri-Voltaggio Zone; sky-blue solid lines are the traces of the vertical cross-sections 1 and 2. b) Vertical cross section (trace 1 on the map) of the relocated seismicity overlayed to a schematic profile by D'Aquisto et al. (2020); the legend is taken from Molli et al. (2010); the green and red solid lines are the Adriatic Moho and Tyrrhenian Moho, respectively, from Di Stefano et al. (2011); the orange solid line is the CSL profile; c) Vertical cross section (trace 2 on the map) showing the 2012 Emilia seismic sequence overlayed to a geological model from the interpretation of an active source seismic profile by Livani et al. (2018): "P.-" are the well locations along our section based on the official coordinates (https://www.videpi.com, last accessed October 2022) and dashed vertical lines are the locations of the same wells along Livani et al. (2018) profile: P. CFEmilia='Castelfranco Emilia' well, P. Spada1='Spada001′ well, P. SFPanaro1='San Felice nel Panaro 1′ well, P. Ficarolo1='Ficarolo 1' well. Solid red stars in a), empty red stars in b) and empty blue stars in c) are M ≥ 5 earthquakes; solid orange circles in a) and empty orange circles in b) and c) are 4 ≤ M < 5 earthquakes; empty black circles are M < 4 earthquakes; black dots are earthquakes with no magnitude attributed in CLASS. (For interpretation of the references to colour in this figure legend, the reader is referred to the web version of this article.)

beneath the Upper Penninic nappes (Alpine units) and the Internal Ligurian Units (Northern Apennines units). On the contrary, most of the seismicity with events that reach magnitude M ≥ 4 (red star in Fig. 7a) is concentrated along the Northern Apennines chain, mainly beneath the External Ligurian Units, the Tuscan nappes (Lunigiana area in map) and in the seismogenic structures buried beneath the Po-Plain sediments (the Mirandola area in Fig. 7).

Trying to investigate the relationship between seismotectonics, lithology and the seismic activity of this area, we present in Fig. 7b a vertical cross section along a representative profile from D'Acquisto et al. (2020). We observe that the large clusters of seismicity beneath the Apuan Alps-Garfagnana and Lunigiana to the SW are essentially enclosed in the continental basement (light gray units in Fig. 7b), and follow the geometry of this unit becoming deeper toward the north-east. On the other hand, in the Reggio Emilia area, the intense seismicity beneath the Mirandola High, largely represented by the 2012 Emilia seismic sequence (Govoni et al., 2014; Scognamiglio et al., 2012), is located above the continental basement and within both the Tuscan nappe and the Tuscan foredeep units (yellow to red colors in Fig. 7b). We also observe constantly present seismicity, although rare and sparse, in the subducting Adriatic lower crust (25 km - 55 km depth).

In Fig. 7c (trace 2 in map) we show some details of the Emilia 2012 seismic sequence located beneath the Mirandola structural high. This sequence was characterized by two mainshocks with Mw 6.1 and 5.9 (Table 1), both with compressive rupture mechanisms. Seismicity distribution is compared with a geologic reconstruction that Livani et al. (2018) obtained by converting in depth a two-way-time (TWT) active-source seismic profile. Because of the difference between the local-scale velocity model used for depth conversion of the seismic profile in Livani et al. (2018) on one hand, and the regional-scale 3D model used for our hypocenter location on the other hand, we note a systematic vertical shift of 2.5 km between seismic event depths and the reconstructed geological model. Thus, taking the position of many wells located along the profiles as reference for the match (Castelfranco Emilia well, Spada1 well, San Felice nel Panaro 1 well, and Ficarolo 1 well in Fig. 7c), we overlay the two images by only imposing a vertical correction of 2.5 km in order to make the two results comparable, while no horizontal shift is applied. Beside the vertical correction, we find a good agreement between the seismicity distribution and both fault system and lithologies reported by Livani et al. (2018). Most of the seismicity occurs within the Norian-Middle Eocene passive margin units, along the basal main SW faults (thick red line in Fig. 7c) while a smaller cluster follows the shallower minor faults beneath the Mirandola town.

The seismicity distribution in the Tuscanian sector of the Northern Apennines is presented in Fig. 8a. This area is characterized by high heat flow (Mongelli and Zito, 2000), shallow Tyrrhenian Moho depth (Piana Agostinetti et al., 2002; Mele and Sandvol, 2003; Di Stefano et al., 2011), asthenosphere uprising beneath the Apennines belt, and geothermal activity in the Larderello area.

The vertical cross section reported in Fig. 8b shows the depth distribution of the seismicity along a profile corresponding to both the SW-NE CROP03 active source seismic line (Pialli et al., 1998) and the lithospheric sketch profile proposed by Chiodini et al. (2004). We observe the presence of the seismically active southwest ward subduction of the Adriatic continental lithosphere evidenced by a well-defined alignment

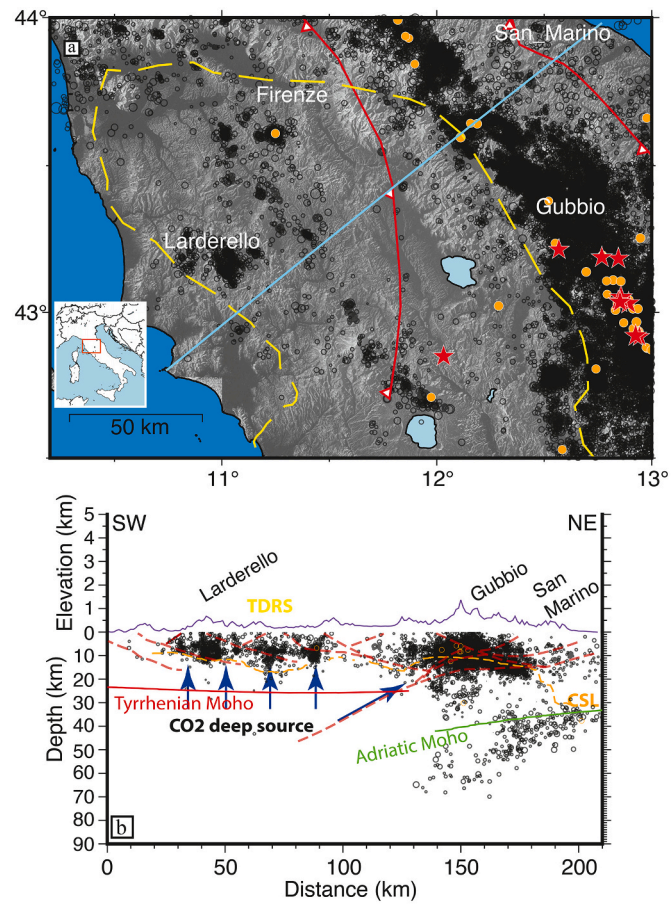

Fig. 8. a) Map view of the seismicity in the Northern Apennines: the yellow dashed line is the contour of the 0.6 probability of deep CO2 source modified after Chiodini et al. (2004); solid red stars are M ≥ 5 earthquakes; solid orange circles are M ≥ 4 earthquakes; open black circles are M < 4 earthquakes; dots are events without attributed magnitude. b) Vertical cross section showing the relocated seismicity along the CROP03 profile reported in Chiodini et al. (2004); the dashed red lines and blue arrows are features modified after Chiodini et al. (2004); the dashed orange line is the CSL profile; the open orange circles are 4 ≤ M < 5 earthquakes; the section includes earthquakes within ±50 km from the trace. (For interpretation of the references to colour in this figure legend, the reader is referred to the web version of this article.)

of hypocenters from 30 km to about 70 km depth in the northeastern part of the section. This seismicity well images with new detail a local shallow Benioff zone that is separated from the local CSL by a volume of very sparse seismicity, denoting a thick layer of lower fragility/higher ductility. This latter evidence, together with the modeled geometry of the Adriatic Moho, might add important information about the recognized crustal delamination process, namely a separation along an inner crustal decollement level of the Adriatic crust, and needs further investigation (Serri et al., 1993; Mantovani et al., 1997; Di Stefano et al., 1999; Di Luzio et al., 2009; Chiarabba et al., 2015; D'Acquisto et al.,

2020).

Chiodini et al. (2004) describe the seismicity distribution in the so-called Tuscan Roman Degassing Structure (TRDS) where seismic activity seems to be strongly influenced by important fluxes of deep source CO_2 measured in the field. The yellow contour in the map of Fig. 8a delimits the area of highest probability of deep source origin for CO_2 fluxes. Despite the large-scale investigation of the present work, the vertical section of Fig. 8b evidences a high level of hypocenter clustering above the TRDS and beneath Tuscany. This seismicity apparently supports, on the long term and at the regional scale, the original hypothesis of Chiodini et al. (2004) that CO_2 of mantle source moves along a pre-existing extensive network of normal faults locally generating overpressure and facilitating earthquakes occurrence.

As suggested by Di Stefano et al. (2009) the broad low-Vp volume imaged by local earthquakes tomography in the Tyrrhenian sea and along the western margin of the Apennines, interpreted as the signature of uprising asthenosphere, represents a reasonable source for the diffuse high heat flow (Mongelli and Zito, 2000) and CO_2 degassing reported in Chiodini et al. (2004). The thermal effect of the up-rising asthenosphere combined with the very thin crust is also responsible for the large distance with no appreciable earthquake hypocenter density in between the CSL and the Tyrrhenian Moho on the Tuscan side, while this cannot be observed beneath the belt above the Adriatic Moho.

5.4. Northern Apennines: The Umbria-Marche sector

In the Umbria-Marche sector of the Northern Apennines, the RSN and other regional permanent networks recorded the most abundant seismicity occurred in Italy in the last 40 years. In particular, the CLASS catalog contains 252,000 earthquakes with more than 207,000 hypocenter locations belonging to classes A and B.

The map view in Fig. 9a shows that the distribution of the relocated seismicity follows the NNW-SSE trend of the Apennines chain. The huge amount of recorded earthquakes is mainly correlated to three seismic sequences (Figs. 9b and d): 1) the 1997–1998 Colfiorito sequence (Amato et al., 1997, Deschamps et al., 2000; Chiaraluce et al., 2003 among many others) with two mainshocks of magnitude Mw 5.7 and Mw 6.0 (section 2 in Fig. 9b), 2) the 2009 L'Aquila sequence (Di Luccio et al., 2010; Chiaraluce et al., 2011 among many others) with a Mw 6.3 mainshock event (section b4 and map view c2 in Fig. 9), and 3) the 2016–2018 Amatrice-Visso-Norcia sequence (Marchetti et al., 2016; Chiaraluce et al., 2017; Improta et al., 2019; Michele et al., 2020 among many others) with two events of Mw 6.2 and Mw 6.6 (section b3 and map view c5 in Fig. 9). In the Umbria-Marche sector of the Apennines, other important sequences and swarms followed moderate magnitude earthquakes, such as the Mw 5.6,1984 Gubbio earthquake (Haessler et al., 1988), the M5.1, 1998 Gualdo Tadino earthquake (Ciaccio et al., 2005), the 2010 Pietralunga sequence (Marzorati et al., 2014), and the 2013–2014 Gubbio swarm (section b1 and map views c3-c4 in Fig. 9, Gualandi et al., 2017).

All the major events occurred along NNW-SSE trending normal faults that accommodate the WSW-ENE tectonic extension (~3–4 mm/yr of horizontal rate, D'Agostino et al., 2008) and dislocate the Oligocene-Quaternary fold-and-thrust belt of the Apennines from Città di Castello to L'Aquila (e.g., Lavecchia et al., 1994; Doglioni et al., 1999; Ghisetti and Vezzani, 2002a, 2002b). Vertical NE-SW cross sections of Fig. 9d illustrate the distribution at depth of the main sequences (coloured symbols) and their spatial relation with the long-term background seismicity (black symbols) from the CLASS catalog. The background seismicity out of the three main seismic sequences is generally characterized by low magnitude earthquakes (only two events with Ml = 4) that are mainly concentrated in a laterally extended zone located at average depths roughly deeper than 8 km and shallower than 16 km depth.

In order to provide a regional scale view of the seismicity evolution, we present in Fig. 9c different map views corresponding to particular temporal ranges that follow or precede the main seismic sequences. Moreover, in Fig. 9d, we propose a space-time plot along a longitudinal NW-SE cross section collapsing events within ±40 km from the profile (events inside the box in Fig. 9a). Colours in both map views (Figs. 9a and c) and space-time plot (Fig. 9d) give information on the hypocentral depths. In particular, we observe that red-to-orange colours well represent both temporal occurrence and duration of the main sequences and swarms. On the other hand, the space-time plot also highlights an almost Continuous Background (CB) seismicity (dark green colours in Figs. 9a, c and d) that persists in all the time range from 1996 to 2018 and roughly occurs beneath 8 km depth as previously remarked in the vertical cross-sections (black dots in Fig. 9b). The spatial distribution over the time of this long-term CB seismicity is mainly enhanced by the map views of Fig. 9c, especially those related to time ranges before and after the 2009 L'Aquila sequence (maps c1 and c4). Long-term CB seismicity distribution along the time axis seems to be different and apparently independent from the discontinuous shallow seismicity related to the major seismic sequences (red and orange dots). For example, the 2009 L'Aquila sequence started south of the CB seismicity limit (purple dashed lines), but developed to the north toward Campotosto, beyond the observed CB seismicity southern limit. On the contrary, the recent 2016–2018 Amatrice-Norcia sequence triggered the deeper seismicity along which many authors identified a subhorizontal seismogenic layer (Michele et al., 2016; Chiaraluce et al., 2017; Vuan et al., 2017; Improta et al., 2019; Michele et al., 2020; Waldhauser et al., 2021 among many others), but not beyond the CB southern limit. It is worth mentioning that some information on a continuous background seismicity in the area was reported by De Luca et al. (2009), although this study was performed over a shorter lapse of time (1981–2006) than that covered by our catalog.

Though with a sparse distribution from 1995 to 2005, and some temporal fluctuations when data from regional networks were not available, the continuity in time of the CB seismicity is confirmed by the impressive event increase from 2012 to 2018, well imaged in the space-time plot, and corresponding to the introduction of the new INGV acquisition system (Margheriti et al., 2021). The image of the CB seismicity remains clearly delimited in the area from Campotosto (CBS southern limit in Fig. 9d and map in Fig. 9a), to Pietralunga (CBS northern limit in Fig. 9d and map in Fig. 9a), although the northern limit seems to be less pronounced than the southern one.

Inset in Fig. 9a (modified after Di Domenica et al., 2014) indicates that the relocated seismicity occurs in a portion of the crust where two major paleogeographic domains of the Adria Mesozoic margin, the Umbro-Marchean Pelagic Basin domain and the Latium-Abruzzi Carbonate Platform domain, come into contact along two important tectonic lines: the Olevano-Antrodoco-Sibillini (OAS) thrust, and the Gran Sasso (GS) thrust, roughly north-south and west-east trending respectively (Barchi et al., 2001; Centamore and Rossi, 2009; Pizzi and Galadini, 2009; Di Domenica et al., 2014 and references therein). Michele et al. (2016) suggested that the OAS and GS oblique thrusts might have played a key role in the evolution of the 2016 Amatrice-Visso-Norcia fault system. Following the paleogeographic reconstruction proposed by Di Domenica et al. (2014), the area south of Campotosto, where the CB seismicity is not observed, roughly corresponds to the Gran Sasso thrust, which marks the transition zone from the pelagic succession of the Umbro-Marchean basin (U-M-S) to the platform-to-slope succession of the Latium-Abruzzi (L-A) domain. According to Barchi et al. (2021) that investigated both the areas of the 1997 Colfiorito and the 2016 Amatrice-Norcia sequences, the subhorizontal basal seismicity, that in our catalog corresponds to the long-term CB seismicity, is observed into the Triassic evaporites unit (the Burano formation, Martinis and Pieri, 1964), mainly composed of anhydrides and dolostones (Trippetta et al., 2010). On the contrary, in both the southern Latium-Abruzzi Carbonate Platform domain and the slope to basin deposits close to the GS thrust, the Triassic evaporites deposits are characterized by a different composition, mainly dolomites (e.g., Cardello and Doglioni, 2015).

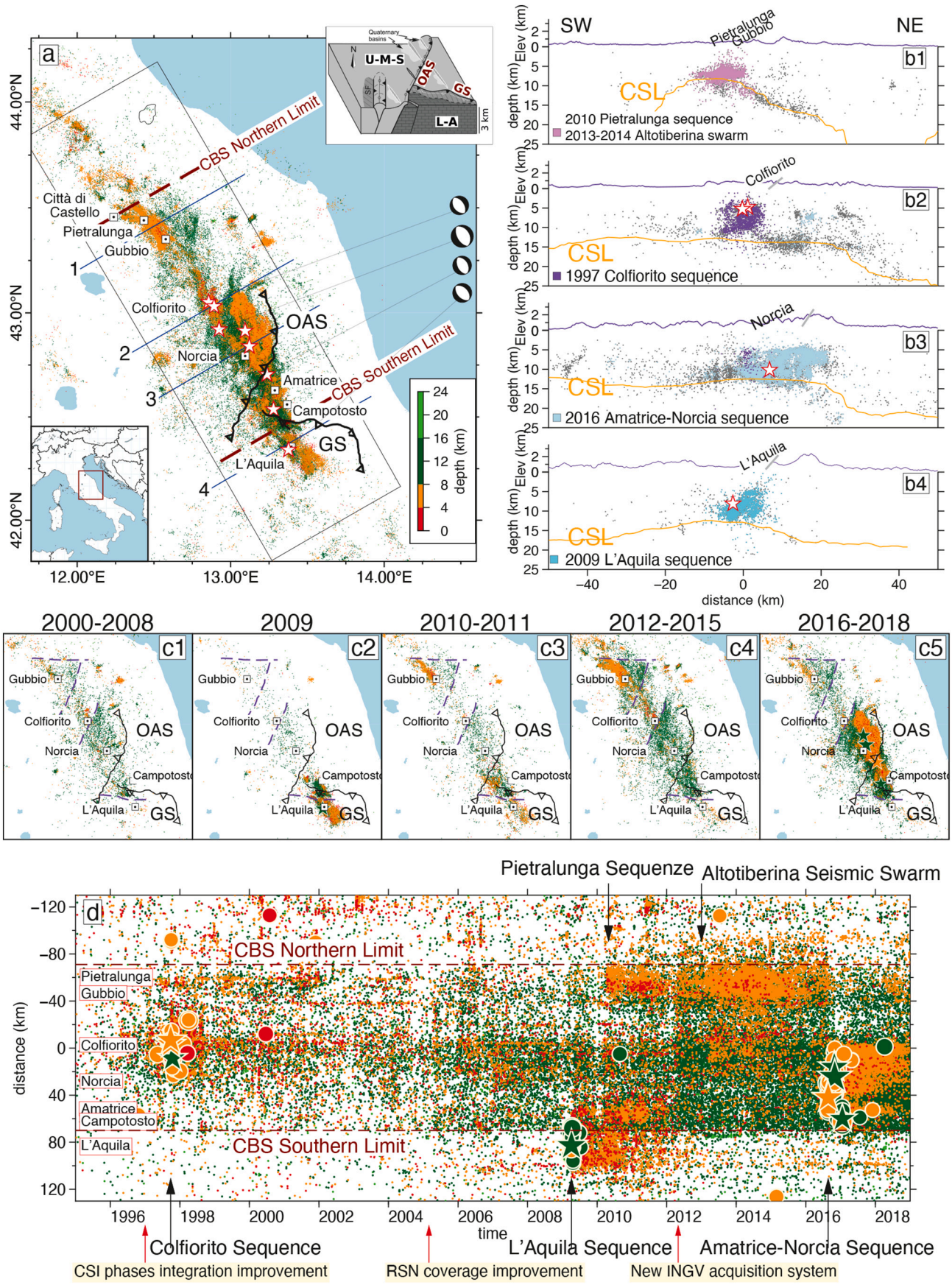

(caption on next page)

Fig. 9. Spatial and temporal distribution of the CLASS seismicity in the Umbria-Marche sector of the Northern Apennines. a) Map view of the relocated earthquakes from 1981 to 2018; coloured dots indicate the hypocenter depths following the colour scale reported in the figure; stars are events with M ≥ 5.5; the two dashed red lines indicate the northern and southern limits of the Continuous Background Seismicity (CBS) described in the text. b) Vertical NE-SW cross sections cutting the Northern Apennines along the major seismic sequences recorded in the last 40 years (the profiles are indicated in the map); coloured symbols are the seismic sequences and swarms discussed in the text, black dots are the hypocenter locations of the long-term background seismicity (CBS); stars are events with M ≥ 5.5, the orange line is the CSL profile; the section includes earthquakes within ±10 km from the trace; c) Map views of the relocated seismicity selected for different time ranges; colours correspond to the scale reported in Fig. 9a). d) Space-time plot of the seismicity projected along a longitudinal NW-SE cross section collapsing events within ±40 km from the profile (hypocenters inside the box of Fig. 9a); event colour code is the same as Fig. 9a; circles are events with 4 ≤ M ≤ 5.5 while stars are events with M ≥ 5.5; the main sequences and seismic swarms discussed in the text are indicated in the plot as well as the three main changement of our catalog due to the INGV acquisition system and the phases integration improvement of the CSI catalog. (For interpretation of the references to colour in this figure legend, the reader is referred to the web version of this article.)

Taking into account this context, we suggest that the long-term CB seismicity distribution might be controlled by the different mechanical behavior of the Triassic deposits belonging to the two paleogeographic domains. Accordingly, the southern limit of the CB seismicity is located some kilometers south of the GS thrust with the same EW orientation (Fig. 9c), possibly indicating the continuation at depth of the Umbria-Marche pelagic sequence beneath the GS thrust, while farther south and beyond the southern limit of the CB the absence of CB seismicity beneath 8 km depth might indicate the presence of the deposits belonging to the Latium-Abruzzi Carbonate Platform domain.

The northward continuity of the CB seems to be interrupted or strongly narrowed in an area well bounded by the two SW-NE purple dashed lines reported in map views of Fig. 9c from Colfiorito to the south of the Alto Tiberina Fault in the Gubbio area. This evidence is difficult to explain without further investigations and deep comparison with seismic lines and geological interpretations but, at least for the southern boundary of this "gap", we notice the presence of the Valnerina Line a few km to the east. This is another important west verging thrust along which stratigraphy abruptly changes and whose behavior and characteristics suggest, according to Tavarnelli et al. (2004), similarly to the OAS, its rooting in the basement. We thus suggest that in the Umbria-Marche sector of the Northern Apennines the presence of a sub-horizontal layer of long-term background seismicity at depth is determined and modulated by the large-scale lateral variation of the main paleogeographic domains, often but not always expressed at surface as inherited thrusts.

5.5. The Northern-Southern Apennines transition zone

The transition from Northern to Southern Apennines is marked by an impressive and abrupt change of earthquake density, moving from NW to SE, as clearly shown in map view (Fig. 10a). The general features of the long-term hypocenter distribution essentially confirm the background seismicity analysis made by Bagh et al. (2007), based on a short-term passive seismology experiment. We observe a deepening of the seismicity from NW to SE, although this deepening, confirmed by our CSL analysis, is slightly higher with respect to previous studies, reaching 25 km depth beneath the Fucino Basin (Fig. 10b).

For this area, Bagh et al. (2007) estimated a constant low seismicity rate of about 2.6 e−04 events/day*km^2 with the exception of few periods characterized by seismic sequences. The authors also hypothesized that the revealed absence of seismicity along defined faults responsible for major earthquakes might be due to a status of locking during an inter-seismic stage. The analysis of our long-term seismicity catalog makes clear that the 2009 L'Aquila seismic sequence filled up the north-western tip of this area. This evidence, together with the much denser seismicity to the SE, has the appearance of a yet large but more delimited volume showing constant low earthquake density and low seismicity rate than that observed in Bagh et al., 2007. This large "gap" corresponds to an area affected by the Mw 7.0, 1915 Marsica earthquake attributed to the Fucino Basin Fault located slightly to the SW.

Moreover, in this zone where the extension occurs on a 50 km wide area (Selvaggi et al., 1997; Bagh et al., 2007), off axis at about 20 km to the NE of the section trace, there is also a second important seismogenic source, the Sulmona Basin Fault, affecting the western flank of Mt. Morrone (Galadini and Galli, 2000; Gori et al., 2011; Di Domenica and Pizzi, 2017). According to Galadini and Galli (2000), the activation of this fault system might give a M 6.5–7.0 earthquake, comparable to the Mw 6.8, 1706 Maiella event (Fig. 10a). Newertheless, the same authors and others later on (Gori et al., 2011; Galli et al., 2015; Di Domenica and Pizzi, 2017) state that this fault cannot be associated with any of the strong historical earthquakes of the region and in particular that the damage distribution of the 1706 earthquake (concentrated in the footwall to the NE of the fault) is not compatible with the fault system. On the basis of field and chronometric dating, Galli et al. (2015) confirm this as a "silent" structure, identifying the last event in the middle of the second century. We here underline the importance, for seismic hazard, of confirming the long-term instrumental seismicity "gap" of this large region hosting well recognized major faults and in particular a fault system, capable of a M 6.5–7.0 earthquake and considered to be silent since about 1.8 ky, in the close vicinity of more recently active faults.

5.6. Southern Apennines

The seismicity in the Southern Apennines is quite differently distributed with respect to the Northern Apennines being essentially confined in a narrow band of about 20 km width in the SW-NE direction, where most of the seismogenic sources reported in the DISS database (DISS Working Group, 2018) are concentrated. This area of Italy was characterized by several strong earthquakes. One of the highest magnitudes and more destructive earthquakes that occurred in Italy in the last 80 years is the M 6.9, 1980 Irpinia earthquake. The complex rupture activated a graben-like fault system with three well constrained main ruptures on distinct fault segments (the NE-dipping Mt. Marzano and Picentini Mountains segments, the NE-dipping San Gregorio Magno fault, and the SW-dipping, antithetic Pescopagano fault), largely discussed and analyzed in literature (Westway and Jackson, 1987; Bernard and Zollo, 1989; Pantosti and Valensise, 1990; Nostro et al., 1997).

In 1996, a second important seismic sequence occurred along this same fault system with a mainshock of Mw 5.1 (ML 4.9) whose location is close to the 20s episode patch area of the 1980 Irpinia earthquake (Cocco et al., 1999; Frepoli et al., 2011). In Fig. 11 we show the seismicity from 1981 to 2018 across this fault system (Figs. 11b-c, sections 1 and 2). It is worth noting that our catalog does not include the 1980 seismic sequence, neither the mainshock nor its early aftershocks, while small magnitude instrumental seismicity in the period 1981–1990 of our catalog is scarce due to the poor network geometry.

To highlight the important relationship between the structures activated by the 1980 seismic sequence and the subsequent 40 years of seismic activity, we overlap our relocated seismicity to a tectonic sketch of the fault system modified after Ascione et al. (2020) that includes the 1980 hypocenter position (white star in Figs. 11b and c, sections 1 and 2). We here distinguish the seismicity of the 1996 sequence from that occurred after. First, we observe that all the seismicity recorded in the last 40 years is still concentrated on this fault system and is distributed from shallow depths to 15-20 km depth. Then, we note that the highest earthquake density is always found along the main Mt. Marzano-Picentini fault and on the Pescopagano antithetic fault (Fig. 11a). The

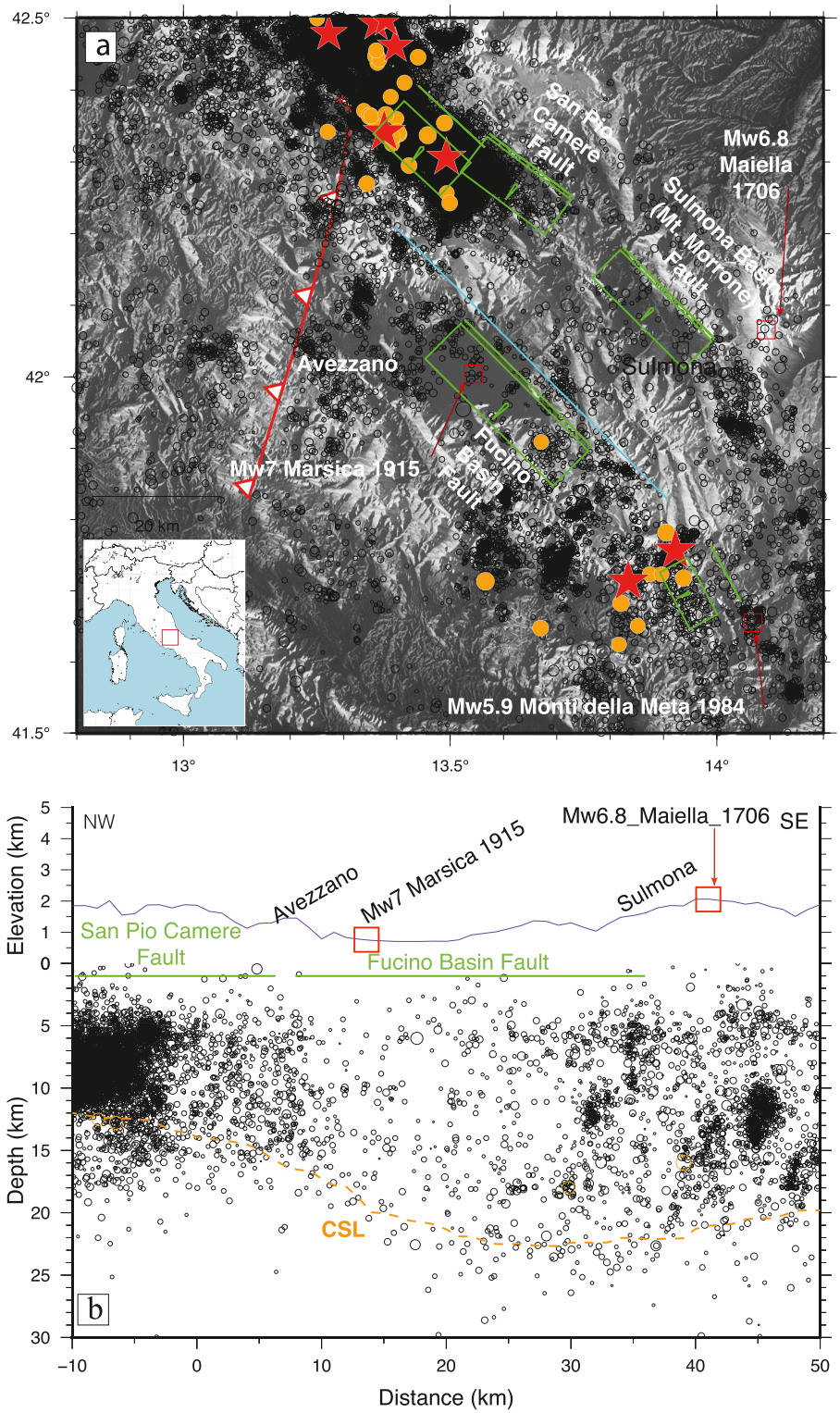

Fig. 10. a) Map view of the seismicity distribution in the Northern-Southern Apennines transition area; green boxes represent the projection of known individual seismogenic sources from the DISS database (DISS Working Group, 2018); red open squares are the location of historical earthquakes from CPTI15 (Rovida et al., 2022; red solid stars are M ≥ 5.0 hypocenters, orange solid circles are 4 ≤ M < 5 hypocenters, open black circles are M < 4 earthquakes, black dots are hypocenters with dimension scaled with respect to their magnitude; the red solid line is the trace of the vertical cross section; b) NW-SE oriented vertical cross section from the southern termination of the 2009 L'Aquila sequence (NW) to the Mw 5.9, 1984 Monti della Meta earthquake (SE). Green horizontal bars indicate the projection of the local seismogenic sources from the DISS database (DISS Working Group, 2018); colors and symbols of the hypocenters are the same as in map view; the orange dashed line is the CSLayer; the open red squares are the projections of historical earthquakes. (For interpretation of the references to colour in this figure legend, the reader is referred to the web version of this article.)

1996 seismic sequence is well visible along the vertical cross section 2 (orange circles and star in Fig. 11c), distributed from the surface to 10 km depth, partly on the southern termination of the Mt. Marzano fault and partly on the northern tip of the San Gregorio Magno fault. Nevertheless, in section 1 this seismic sequence seems to mainly activates the deep fault from 4 to 10 km depth, slightly shifted with respect to the surface outcropping fault, according to Ascione et al. (2020). In section 2 (Fig. 11c) on the contrary, the San Gregorio Magno fault shows the 1996 seismicity mostly limited to the shallower depths from 0 to 5 km. A final observation is that, according to our catalog selected for qualities A and B, the seismicity from 1997 to 2018 is also densely distributed at depths below the 1980 earthquake hypocenter, at the convergence between the main NE dipping faults and the antithetic fault and close to the very shallow fault branches reported in the Ascione et al. (2020) geologic scheme.

Longitudinal section (Fig. 11e) extending to the Val D'Agri Fault

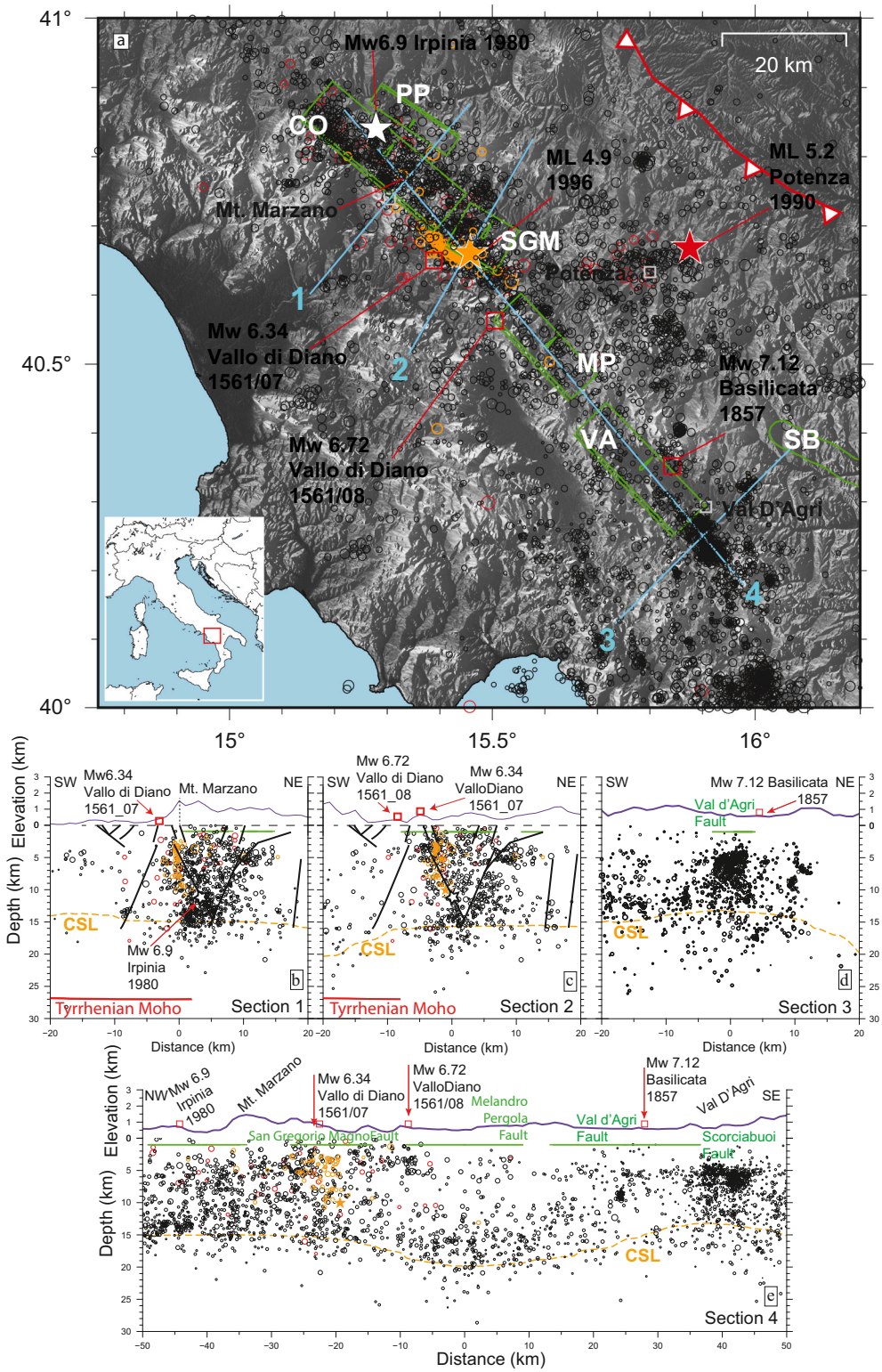

Fig. 11. CLASS seismicity distribution in the southern Apennines in map view (a) and 4 vertical cross sections (b, c, d, e); open red circles are the M < 5, 1981–1995 earthquakes, open orange circles are the M < 5, 1996 earthquakes, open black circles are the M < 5, 1997–2018 earthquakes, red open squares are historical earthquakes (from Rovida et al., 2022); skyblue solid lines in map are the traces of the vertical sections; green boxes in map and green solid lines in vertical sections are the following individual seismic sources according to DISS: PP=Pescopagano, CO=Colliano, SGM = San Gregorio Magno, MP = Melandro-Pergola, VA = Val d'Agri, and SB=Scorciabuoi; the white star both in map and in the vertical sections 1 and 2 is the location of the Mw 6.9, 1980 Irpinia event from the sketch by Ascione et al. (2020) that we also reported modified as a structural reference in vertical sections 1 and 2; the orange dashed line in the vertical sections is the trace of the CSL. (For interpretation of the references to colour in this figure legend, the reader is referred to the web version of this article.)

system, highlights how seismicity here is scarce and mostly concentrated at depth, except for the Mw 5.8, 1990 Potenza seismic sequence (Table 1), which is located toward NE, about 30 km off the axis of the section. This long-term shallow depth "gap" roughly corresponds to the location of two historical earthquakes: the Mw 6.7, 1561 Vallo di Diano earthquake and the Mw 7.1, 1857 Basilicata earthquake to the NW and to the SE respectively. This "gap" is bordered to SE by the Val D'Agri seismicity (see sections 3 and 4), whose distribution is in good agreement with that described in much finer details in Valoroso et al., 2009. Section 3 also shows a peculiar distribution of the Val D'Agri seismicity that is very scarce to the NE, from 10 km to 20 km along the section. Based on geological evidence in this region, some authors hypothesized the presence of a 30 km long WNW-ESE trending fault, the "Scorciabuoi fault" (green trace in the map), initially formed as an oblique-lateral ramp, and then inverted and reactivated as a normal fault (Catalano et al., 1993; Pieri et al., 1994; Pieri et al., 1997; Casciello

et al., 2002; Patacca and Scandone, 2001). Despite the absence of historical earthquakes, the existence of a late Pleistocene activity of this fault was recently confirmed through a multidisciplinary geological and geophysical study (Caputo et al., 2007). We therefore hypothesize that the scarce seismic activity here reported in our catalog might be related to this fault, essentially at depth while its shallow part is mostly silent.

5.7. Calabrian Arc

As previously summarized, both subduction and continental collisions shaped the entire Italian peninsula (Fig. 1). Geophysical signatures of the subducting plates, in terms of seismic velocity anomalies, are well visible down to hundreds of kilometers depth beneath both the Northern Apennines and the Calabrian Arc. Nevertheless, only beneath this latter, the subducting slab is outlined by the seismicity distribution, allowing us to define its lateral and vertical thickness and its geometry variations.

We present six vertical cross sections from azimuth N50° to N150° with 20° steps, almost always orthogonal to the dipping plate curvature. Our images highlight at least three important features: 1) the slab is seismically active, with continuous spatial distribution defined from shallow to higher depths, only in its central part, i.e., from section 3 (Fig. 12d) to section 5 (Fig. 12f) close the Messina strait (Sicily); 2) outside this zone of the Calabrian Arc (Figs. 12b and g), the seismicity distribution depicts a fragmented plate with an upper portion almost continuous down to about 80 km depth, and a deeper portion below 100 km depth that in section 1 appears limited to a small fragment below 250 km depth; 3) where the tips of the two fragments come into contact around 100 km depth, this junction is characterized by a knee (see open purple diamond in Fig. 12c) and a much higher density of earthquakes of moderate to small magnitude.

It is worth noting that a well defined geometry with lateral continuity of the Ionian subducting lithosphere is only present down to about 80 km depth. This limit also represents the maximum depth of the subduction-related seismicity in the Northern Apennines (Fig. 7b). The high concentration of earthquakes and the knee geometry at about 80–100 km depth suggest that this limit might represent a key zone for the Italian subduction "sensu latu" (i.e., in Northern Apennines and Calabrian Arc) where the slab undergoes a concentration of both stress and deformation and/or specific lithosphere weakness, leading to the well imaged and widely discussed slab detachment (see Wortel and

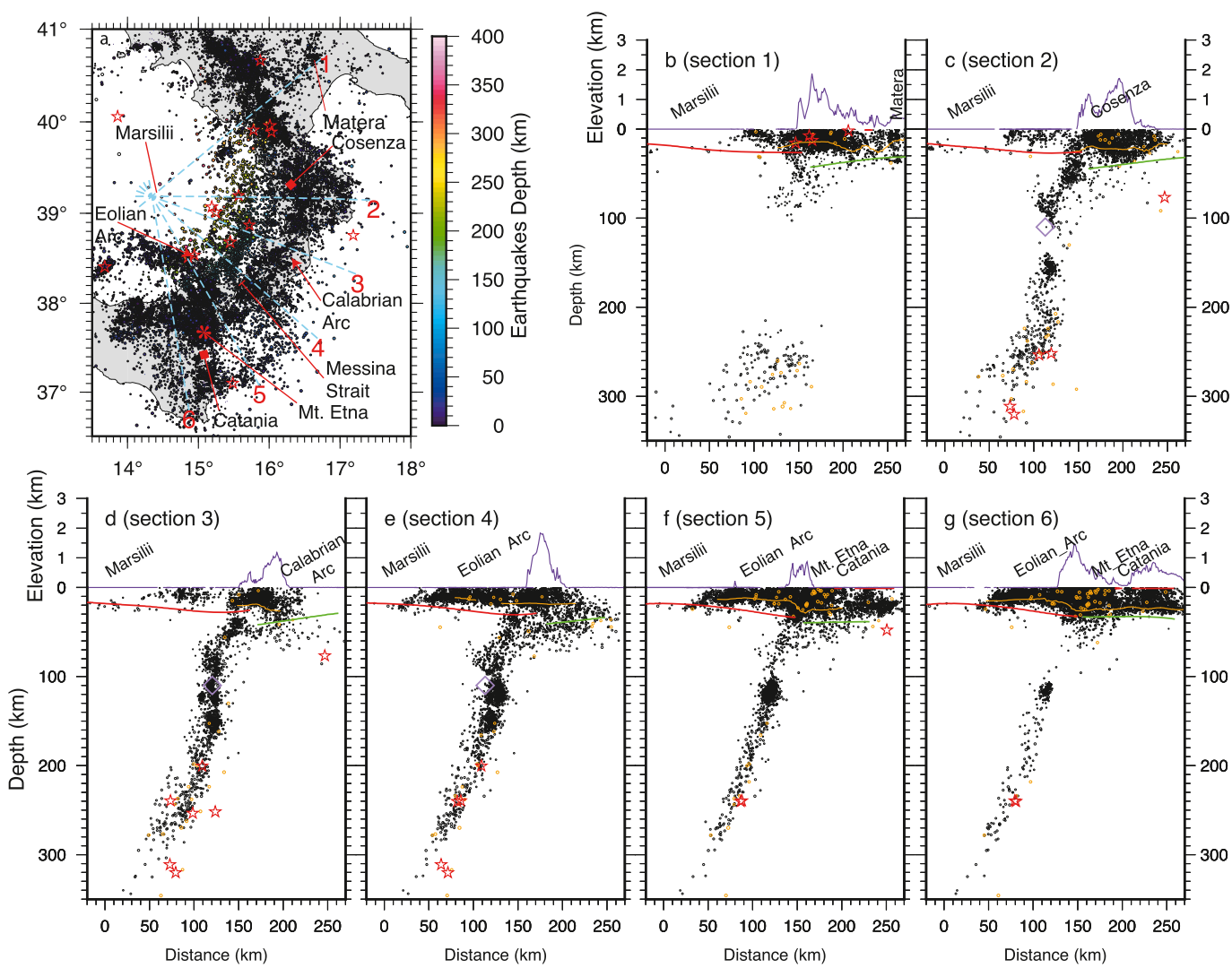

Fig. 12. a) Distribution in map of A to C quality earthquakes in the Southern Tyrrhenian region; sky blue dashed lines are the traces of the vertical sections that roughly cut the area orthogonal to the slab curvature, open red stars represent the M ≥ 5.0 earthquakes, coloured circles are M < 5.0 earthquakes scaled with M and coloured by depth (see the colour scale); b-g) vertical sections from 1 to 6 reported in map; open black circles are M < 4 earthquakes scaled with M, open orange circles are 4 ≤ M < 5.0 earthquakes, open red stars are M ≥ 5.0 earthquakes, the orange solid line is the CSL, red solid line is the Tyrrhenian Moho, green solid line is the Adriatic/Ionian Moho, the open purple diamond is the approximate location of the knee as discussed in the text. (For interpretation of the references to colour in this figure legend, the reader is referred to the web version of this article.)

Spakman, 1992, Wortel and Spakman, 2000, Gvirtzman and Nur, 1999, Lucente et al., 1999, Montuori et al., 2007; Chiarabba et al., 2008; Scarfì et al., 2018 among many others). This tearing detachment is discussed in detail in a recent tomographic study by Scarfì et al. (2018) where the authors also focus on the knee at about 100–150 km depth and compare their relocated seismicity to the resulting velocity model. Nevertheless, in the present paper, we use a much higher number of well constrained locations allowing us to image the seismically active volume of the Ionian lithosphere in all its lateral and depth extension at a higher level of detail. This allows us to notice that the break at 80 km depth is abrupt (see Figs. 12b and d, sections 1 to 3) and corresponds to a visible change in the plate dip. The shallow fragment of the imaged plate shows almost constantly a 55° dip, while the deeper fragment has a variable dip ≥70°. From this evidence we might argue that the shallow part of the plate has a strongly stable equilibrium represented by a constant geometry and the deeper part is evidently sinking. Therefore we hypothesize that, where the break is at the initial stage at about 80–100 km depth (namely at the two lateral tips of the continuous portion of the slab, central Calabrian Arc and Eastern Sicily), there is a concentration of strain leading to the observed higher density of earthquakes.

Regarding the shallow sub-horizontal portion of the subducting Ionian plate, recent new seismological evidences based on the analysis of changes in the depth distribution of earthquakes (Sgroi et al., 2021) suggest that the Ionian Fault (IF in Fig. 13) is a major lithospheric boundary separating an "Eastern Lobe" (northeast of the IF trace) and a "Western Lobe" (southwest of the IF trace) of the Ionian accretionary wedge (Polonia et al., 2011, 2016) characterized by higher and lower thickness of the seismogenic layer respectively. The region located

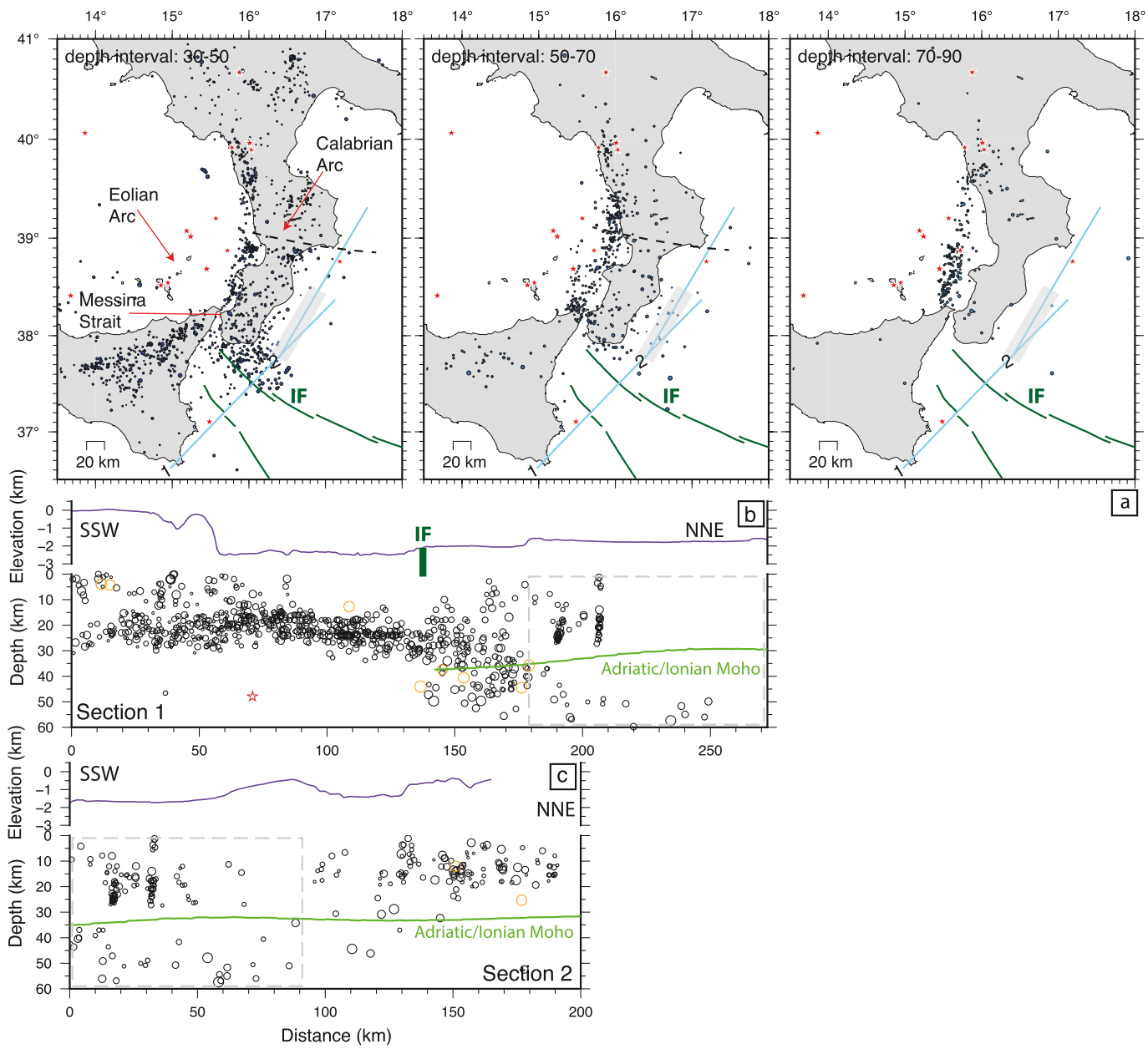

Fig. 13. a) Distribution of the CLASS relocated hypocenters with quality class from A to C, within ±10 km around 40, 60, 80 km depth layers: both depth colour scale and magnitude symbols are the same as in Fig. 12. The solid sky-blue lines are the traces of vertical sections 1 and 2; the gray-shaded segment along section 2 corresponds to the dashed gray boxes in sections 1 and 2 (b and c); IF is the surface trace of the Ionian Fault (Sgroi et al., 2021); the dashed black line is the hypothetic northern limit of the deep seismicity; b) distribution of CLASS hypocenters in vertical section 1, IF is the intersection of the Ionian Fault with section 1; c) distribution of CLASS hypocenters in vertical section 2; in both sections 1 and 2 the green solid line is the Adriatic/Ionian Moho and the purple solid line is the bathymetry of the Ionian Sea. (For interpretation of the references to colour in this figure legend, the reader is referred to the web version of this article.)

northeast of the IF is considered involved in thick-skinned tectonics probably due to a link between deep processes and shallow structural development as suggested by Sgroi et al. (2021).

In order to investigate the lateral extension of this evidenced thick-skinned tectonics, we plot in Fig. 13 the CLASS hypocenter locations in horizontal slices cutting the earthquake distribution at different depth intervals from 30 km to 90 km with 20 km thickness step intervals, as well as two partially overlapping cross-sections. Section 1 corresponds to the vertical section B—B1 reported in Sgroi et al. (2021), while section 2 is its prosecution toward NE, parallel to the Calabrian arc. By comparing the horizontal depth layers and the vertical sections 1 and 2, we suggest that this thick-skinned tectonics behavior is limited to a ~ 130 km large area to the north-east of the Ionian Fault, whose limit might be represented by the black solid line in Fig. 13a (map views at 30–50 km depth, and 50–70 km depth). This zone roughly corresponds to the area of larger vertical continuity of the slab (Fig. 12) supporting the above-mentioned hypothesis of deep processes influencing the shallow tectonics in this area.

6. Conclusions

The 1981–2018 CLASS catalog presented in this work is the result of a two-steps process. The first one consisted in collecting an integrated dataset of ~5.0 million P- and ~ 3.5 million S-wave arrival times recorded by the Italian National Seismic Network and other permanent seismological networks. The second one consisted in relocating the hypocenters of the whole dataset following a probabilistic approach and using the non-linear program NonLinLoc with updated 3D, P and S velocity models of Italy. By applying an empirical quality classification method to more than 400,000 hypocenter solutions, we produced a high-quality selected dataset of seismicity that covers an extended instrumental seismological epoch from 1981 to 2018 (about 40 year), providing a high resolution, large-scale image of the 3D earthquake distribution in Italy.

The possibility to observe the long-term behavior of the seismic activity in Italy is one of the more relevant aspects of the present work leading to two major results.

Regarding our first result, the well located seismicity combined with the use of the Moho discontinuity for crustal earthquake selection allowed us to perform a complete and high resolution computation of the Crustal Seismogenic Layer (CSL). Our new map evidenced CSL depth variations at regional and local scale. Higher depths are imaged in the Adriatic domain: since the analysis of the ratio between the CSL and the Moho depths (CM ratio) shows that in most of the cases the CSL depth is proportional to the Moho depth with a CM in the range 0.4–0.6 in both the Tyrrenian and Adriatic domains, we might suggest that the regional scale variation of the CSL in Italy is on average correlated to the crustal thickness. The analysis of the CM ratio was also useful to discriminate real anomalies in CSL depths, here identified where the CM ratio exceeds 0.6 or is lower than 0.4. An interesting example of such areas is located in the Adriatic side of the Southern Apennines, where the presence of strike slip fault systems characterizes the local strain regime with structures extending to the lower crust. This behavior corresponds to CM ratio values higher than 0.8 on a wide area. A detailed geographical analysis of the high frequency variations of both the CSL depth and the CM ratio might lead to specific future studies.

Our second major result concerns the time-space homogeneities of the CLASS catalog over such a long time span that allowed us to produce a general overview of the 3D seismicity distribution in Italy from the Alps to the Calabrian Arc, evidencing large or small scale features depending on the contribution given by our results.

In the Alps, CLASS confirms that the seismicity is essentially distributed along the main tectonic lines. In the Western Alps it is driven at depth by the tectonic contact between internal and external units, namely the Penninic Front, while in the Eastern Alps a general clustering is observed close and along the maximum curvature of the South Alpine Thrust and the Insubric-Periadriatic Lines, marking the tectonic contact between the Northern and the Southern Alps.

In the Tuscan-Emilian part of the Northern Apennines, the large clusters of seismicity seem to follow the geometry of the continental basement becoming deeper (down to ~25 km depth) toward the north-east, beneath the mountain chain of the Apuan Alps. Deep seismicity (more than ~25 km depth) is very scarce, beneath the chain and also within the flexed Adriatic lithosphere. Conversely, the deep seismicity is confirmed to the south in the Tuscan area of the Northern Apennines where it represents the signature of the Adriatic lithosphere subduction. Moreover, in this area, the CM ratio shows a slight band of very low values ($0.2 < CM < 0.4$) where the CSL is essentially related to the seismicity in the upper Adriatic crust and appears very far from the Adriatic Moho flexed below. This feature is probably due to crustal delamination processes. On the contrary, the distribution of seismicity is almost totally confined above 15 km depth on the Tyrrhenian side. This corresponds to the presence of a low-Vp volume interpreted by several authors as the signature of up-rising asthenosphere and a source for the diffuse high heat flow and CO_2 degassing reported in this area. These features combined with the very thin crust, are the cause for the seismic activity confined at very shallow depths.

An important part of the seismicity of our catalog (about 250,000 earthquakes) is located in the Umbria-Marche sector of the Northern Apennines. This huge amount of earthquakes is mainly associated with the three major seismic sequences of the last 25 years: the 1997–1998 Colfiorito sequence, the 2009 L'Aquila sequence, and the 2016–2018 Amatrice-Visso-Norcia sequence (Table 1). Thanks to the long-lasting catalog and the improved earthquake locations, we identify an intense and almost Continuous Background (CB) seismicity that persists, independently from the evolution of the major seismic sequences, at least in the time range from 1996 to 2018. CB seismicity roughly occurs beneath ~8 km depth along a sub-horizontal distribution that covers a wide region from Pietralunga (north) to Campotosto (south). Taking into account the paleogeographic models of the Northern Apennines, we suggest that this long-lasting, subhorizontal background seismicity might be determined and modulated by the large-scale lateral variation and the different mechanical behavior of the Triassic deposits belonging to the Umbria-Marchean Pelagic basin domain and the Latium-Abruzzi Carbonate platform domain.

In the transition zone from the Northern to the Southern Apennines, south of the 2009 L'Aquila seismic sequence, we confirm the increasing of the CSL depth and a persistent "gap", more precisely definable as a volume with very low seismicity rate, over a 50 km wide area in the instrumental recording period from 1981 to 2018. This is an important aspect that we have discussed in the light of our integrated and relocated catalog, also considering that this area hosted strong historical earthquakes and a potentially seismogenic structure considered by many authors as silent. Another area of relatively scarce seismicity, here limited to the shallow part above 10 km depth, is evidenced in CLASS in the Southern Apennines, where two historical earthquakes with $M > 6.5$ occurred in 1561 and 1857. To the north of this sector of the Apennines we focused on the image restituted by CLASS in the aftermath of the strongest 1980, M 6.9 Irpinia earthquake whose aftershocks are not included in our catalog. It is worth noting that after about 40 years, the seismicity of this area is still mostly concentrated in a narrow band, especially in correspondence with the complex faults system activated by the 1980 Irpinia earthquake.

In the Calabrian Arc area, which is dominated by the Ionian plate subduction, our catalog contributes defining the lateral and vertical thickness of the slab as well as its geometry variations with a resolution higher than previous studies. Based on the recorded instrumental seismicity reported in our vertical cross-sections, we notice that the Ionian slab extending down to at least 400 km depth is horizontally and vertically continuous only from the middle part of the Calabrian Arc to the eastern Sicily. Outside this area, the continuity of the seismicity is limited to about 80 km depth. We observe that this limit is similar to the

depth extent of the subduction-related seismicity in the Northern Apennines. Moreover, our results show that the continuous part of the slab is characterized by a volume having a much higher density of earthquakes around 100 km depth and a "knee" marking an abrupt change of the slab dip. Taking into account these two main observations, we suggest that the limit of 80 km might be a key depth for the subduction of the Adriatic-Ionian lithosphere, where the subducting slab undergoes a concentration of deformation possibly due to a specific lithosphere weakness that leads to the slab detachment widely discussed in literature.

The results of our work, briefly presented and discussed in this paper and here summarized in the conclusions, allow us to validate our approach and support further applications of the CLASS catalog that is available for the scientific community and can be used as an input for further studies of double differences earthquake relocations or 3D travel time tomographies at regional scale. Moreover, future steps involving a new computation of earthquake magnitudes over the time can provide an updated homogeneous catalog for hazard studies.

CRediT authorship contribution statement

Diana Latorre: Conceptualization, Investigation, Software, Validation, Formal analysis, Visualization, Writing original and revised drafts.

Raffaele Di Stefano: Conceptualization, Investigation, Software, Validation, Visualization, Writing original and revised drafts.

Barbara Castello: Conceptualization, Data curation, Writing original and revised drafts.

Maddalena Michele, Conceptualization, Software, Data curation, Visualization, Writing - original draft and revised drafts.

Lauro Chiaraluce: Conceptualization, Project administration, Funding acquisition, Writing original and revised drafts.

Declaration of Competing Interest

The authors declare that they have no known competing financial interests or personal relationships that could have appeared to influence the work reported in this paper.

Data availability

CLASS hypocenter locations are available at https://doi.org/10.13127/class.1.0. The CLASS integrated phases dataset 1981-2008 is available at https://doi.org/10.13127/csi.2.0/phs as CSI 2.0/phases. CLASS phases for the period 2009-2014 are available at https://doi.org/10.13127/ISIDE. CLASS phases for the period 2015-2018 are available at http://terremoti.ingv.it/bsi.

Acknowledgment

Figures are generated by The Generic Mapping Tools (GMT) by Wessel et al., 2019. The catalog benefits from the long-lasting, tireless products of many routine analysis seismologists both from INGV and from other institutions. We thank the Editor and the two anonymous reviewers for their constructive comments that have improved the manuscript. This study was funded by the Italian Presidenza del Consiglio dei Ministri–Dipartimento della Protezione Civile (DPC) "Obiettivo 2 Accordo Quadro 2012- 2021 DPC-INGV - Convenzione B2", and by the RISE (Real-time Earthquake Risk Reduction for a Resilient Europe) project under the European Union's Horizon 2020 research and innovation programme (grant agreement No 821115).

Appendix A. Supplementary data

Supplementary data to this article can be found online at https://doi.org/10.1016/j.tecto.2022.229664.

References

Amato, A., Azzara, R., Chiarabba, C., Cimini, G.B., Cocco, M., Di Bona, M., Margheriti, L., Mazza, S., Mele, F., Selvaggi, G., Basili, A., Boschi, E., Courboulex, F., Deschamps, A., Gaffet, S., Bittarelli, G., Chiaraluce, L., Piccinini, D., Ripepe, M., 1997. The 1997 Umbria-Marche, Italy, earthquake sequence: a first look at the main shocks and aftershocks. Geophys. Res. Lett. 25, 2861–2864. https://doi.org/10.1029/98GL51842.

Argand, E., 1924. La tectonique de l'Asie. Comptes Rendus Congrés Géologique International, XIII, Belgique 1922 (1), 171–372.

Ascione, A., Nardò, S., Mazzoli, S., 2020. The M_S 6.9, 1980 Irpinia earthquake from the basement to the surface: a review of tectonic geomorphology and geophysical constraints, and new data on postseismic deformation. Geosciences 10. https://doi.org/10.3390/geosciences10120493.

Bagh, S., Chiaraluce, L., De Gori, P., Moretti, M., Govoni, A., Chiarabba, C., Di Bartolomeo, P., Romanelli, M., 2007. Background seismicity in the Central Apennines of Italy: the Abruzzo region case study. Tectonophysics 444, 80–92. https://doi.org/10.1016/j.tecto.2007.08.009.

Barchi, M., Landuzzi, A., Minelli, G., Pialli, G., 2001. Outher Northern Apennines. In: Vai, G.B., Martini, I.P. (Eds.), Anatomy of an Orogen: The Apennines and Adjacent Mediterranean Basin. Kluwer Publishers, London, pp. 215–254. https://doi.org/10.1007/978-94-015-9829-3.

Barchi, M.R., Carboni, F., Michele, M., Ercoli, M., Giorgetti, C., Porreca, M., Azzaro, S., Chiaraluce, L., 2021. The influence of subsurface geology on the distribution of earthquakes during the 2016–2017 Central Italy seismic sequence. Tectonophysics 807, 228797. https://doi.org/10.1016/j.tecto.2021.228797.

Bernard, P., Zollo, A., 1989. The Irpinia (Italy) 1980 earthquake: detailed analysis of a complex normal faulting. J. Geophys. Res. Solid Earth 94, 1631–1647. https://doi.org/10.1029/JB094iB02p01631.

Bethoux, N., Theunissen, T., Beslier, M.O., Font, Y., Thouvenot, F., Dessa, J.X., Simon, S., Courrioux, G., Guillen, A., 2016. Earthquake relocation using a 3D a-priori geological velocity model from the western Alps to Corsica: Implication for seismic hazard. Tectonophysics 670, 82–100. https://doi.org/10.1016/j.tecto.2015.12.016.

Bousquet, R., Schmid, S.M., Zeilinger, G., Oberhänsli, R., Rosenberg, C., Molli, G., Robert, C., Wiederkehr, M., Rossi, Ph., 2012. Tectonic Framework of the Alps (CCGM/CGMW).

Calais, E., Nocquet, J.M., Jouanne, F., Tardy, M., 2002. Current strain regime in the western Alps from continuous global positioning system measurements, 1996–2001. Geology 7, 651–654. https://doi.org/10.1130/0091-7613(2002)030<0651:CSRITW>2.0.CO;2.

Callegari, E., Brack, P., 2002. Geological map of the tertiary adamello batholith (Northern Italy) Explanatory notes and legend. Mem. Sci. Geol 54. ISSN 0391-8602.

Capitanio, F.A., Goes, S., 2006. Mesozoic spreading kinematics: Consequences for Cenozoic Central and Western Mediterranean subduction. Geophys. J. Int. 165, 804–816. https://doi.org/10.1111/j.1365-246X.2006.02892.x.

Caputo, R., Salviulo, L., Piscitelli, S., Loperte, A., 2007. Late Quaternary activity along the Scorciabuoi Fault (Southern Italy) as inferred from electrical resistivity tomographies. Ann. Geophys. 50 https://doi.org/10.4401/ag-3078.

Cardello, G.L., Doglioni, C., 2015. From mesozoic rifting to Apennine orogeny: the gran Sasso range (Italy). Gondwana Res. 27 (4), 1307–1334.

Casciello, E., Pappone, G., Zuppetta, A., 2002. Structural features of a shear-zone developed in an argillaceous medium: the southern portion of the Scorciabuoi fault (southern Apennines). Bollettino della Società Geologica Italiana, Volume Speciale 1 (2), 659–667.

Castello, B., Selvaggi, G., Chiarabba, C., Amato, A., 2006. CSI Catalogo della sismicità italiana 1981–2002, versione 1.1. INGV-CNT, Roma doi. https://doi.org/10.13127/CSI.1.1.

Castello, B., Olivieri, M., Selvaggi, G., 2007. Local and duration magnitude determination for the Italian earthquake catalogue (1981-2002). Bull. Seismol. Soc. Am. 97, 128–139. https://doi.org/10.1785/0120050258.

Catalano, S., Monaco, C., Tortorici, L., Tansi, C., 1993. Pleistocene strike-slip tectonics in the Lucanian Apennine (southern Italy). Tectonics 12 (3), 656–665. https://doi.org/10.1029/92TC02251.

Centamore, E., Rossi, D., 2009. Neogene-Quaternary tectonics and sedimentation in the Central Apennines. Boll. Soc. Geol. Ital. 128, 73–88.

Chiarabba, C., De Gori, P., 2016. The seismogenic thickness in Italy: constraints on potential magnitude and seismic hazard. Terra Nova 28.

Chiarabba, C., Jovane, L., DiStefano, R., 2005. A new view of Italian seismicity using 20 years of instrumental recordings. Tectonophysics 395, 3–4.

Chiarabba, C., De Gori, P., Speranza, F., 2008. The southern Tyrrhenian subduction zone: deep geometry, magmatism and Plio-Pleistocene evolution. Earth Planet. Sci. Lett. 268, 3–4.

Chiarabba, C., De Gori, P., Mele, F.M., 2015. Recent seismicity of Italy: active tectonics of the Central Mediterranean region and seismicity rate changes after the Mw 6.3 L'Aquila earthquake. Tectonophysics 638, 82–93. https://doi.org/10.1016/j.tecto.2014.10.016.

Chiaraluce, L., Ellsworth, W.L., Chiarabba, C., Cocco, M., 2003. Imaging the complexity of an active normal fault system: the 1997 Colfiorito (Central Italy) case study. J. Geophys. Res. 108, 2294. https://doi.org/10.1029/2002JB002166, B6.

Chiaraluce, L., Valoroso, L., Piccinini, D., Di Stefano, R., De Gori, P., 2011. The anatomy of the 2009 L'Aquila normal fault system (Central Italy) imaged by high resolution foreshock and aftershock locations. J. Geophys. Res. 116, B12311. https://doi.org/10.1029/2011JB008352.

Chiaraluce, L., Di Stefano, R., Tinti, E., Scognamiglio, L., Michele, M., Casarotti, E., Cattaneo, M., De Gori, P., Chiarabba, C., Monachesi, G., Lombardi, A., Valoroso, L., Latorre, D., Marzorati, S., 2017. The 2016 Central Italy Seismic Sequence: a first look

at the Mainshocks, aftershocks, and Source Models. Seismol. Res. Lett. 88, 757–771. https://doi.org/10.1785/0220160221.
Chiodini, G., Cardellini, C., Amato, A., Boschi, E., Caliro, S., Frondini, F., Ventura, G., 2004. Carbon dioxide Earth degassing and seismogenesis in central and southern Italy. Geophys. Res. Lett. 31, L07615. https://doi.org/10.1029/2004GL019480.
Ciaccio, M., Cimini, G., Amato, A., 1998. Tomographic images of the upper mantle high-velocity anomaly beneath the northern Apennines. Mem. Soc. Geol. Ital. 52, 353–364.
Ciaccio, M., Barchi, M., Chiarabba, C., Mirabella, F., Stucchi, E., 2005. Seismological, geological and geophysical constraints for the Gualdo Tadino fault, Umbria–Marche Apennines (central Italy). Tectonophysics 406, 233–247. https://doi.org/10.1016/j.tecto.2005.05.027.
Ciaccio, M.G., Di Stefano, R., Improta, L., Mariucci, M.T., BSI Working Group, 2021. First-Motion Focal Mechanism Solutions for 2015–2019 M $\geq$ 4.0 Italian Earthquakes. Front. Earth Sci. 9, 630116 https://doi.org/10.3389/feart.2021.630116.
Cimini, G.B., De Gori, P., 2001. Nonlinear P-wave tomography of subducted lithosphere beneath central-southern Apennines (Italy). Geophys. Res. Lett. 28, 4387–4390. https://doi.org/10.1029/2001GL013546.
Cocco, M., Chiarabba, C., Di Bona, M., Selvaggi, G., Margheriti, L., Frepoli, A., Lucente, F. P., Basili, A., Jongmans, D., Campillo, M., 1999. The April 1996 Irpinia seismic sequence: Evidence for fault interaction. J. Seismol. 3, 105–117. https://doi.org/10.1023/A:1009771817737.
CSTI working group, 2001. Catalogo Strumentale dei Terremoti Italiani dal 1981 al 1996, Progetto GNDT, sottoprogetto 5.1.3, AA.VV.
CSTI Working Group, 2005. Catalogo Strumentale dei Terremoti Italiani dal 1981 al 1996 (Versione 1.1). https://emidius.mi.ingv.it/CSTI/Versione1_1.
D'Acquisto, M., Dal Zilio, L., Molinari, I., Kissling, E., Gerya, T., van Dinther, Y., 2020. Tectonics and seismicity in the Northern Apennines driven by slab retreat and lithospheric delamination. Tectonophysics 789, 228481. https://doi.org/10.1016/j.tecto.2020.228481.
D'Agostino, N., Selvaggi, G., 2004. Crustal motion along the Eurasia-Nubia plate boundary in the Calabrian Arc and Sicily and active extension in the Messina Straits from GPS measurements. J. Geophys. Res. Solid Earth 109 (B11). https://doi.org/10.1029/2004JB002998.
D'Agostino, N., Giuliani, R., Mattone, M., Bonci, L., 2001. Active crustal extension in the central Apennines (Italy) inferred from GPS measurements in the interval 1994–1999. Geophys. Res. Lett. 28, 2121–2124. https://doi.org/10.1029/2000GL012462.
D'Agostino, N., Cheloni, D., Mantenuto, S., Selvaggi, G., Michelini, A., Zuliani, D., 2005. Strain accumulation in the southern Alps (NE Italy) and deformation at the northeastern boundary of Adria observed by CGPS measurements. Geophys. Res. Lett. 32, L19306. https://doi.org/10.1029/2005GL024266.
D'Agostino, N., Avallone, A., Cheloni, D., D'Anastasio, E., Mantenuto, S., Selvaggi, G., 2008. Active tectonics of the Adriatic region from GPS and earthquake slip vectors. J. Geophys. Res. 113, 19. https://doi.org/10.1029/2008JB005860.
D'Agostino, N., D'Anastasio, E., Gervasi, A., Guerra, I., Nedimović, M.R., Seeber, L., Steckler, M., 2011. Forearc extension and slow rollback of the Calabrian Arc from GPS measurements. Geophys. Res. Lett. 38 https://doi.org/10.1029/2011GL048270.
De Luca, G., Cattaneo, M., Monachesi, G., Amato, A., 2009. Seismicity in central and northern Apennines integrating the Italian national and national network. Tectonophysics 476, 121–135. https://doi.org/10.1016/j.tecto.2008.11.032.
Delacou, B., Sue, C., Champagnac, J.-L., Burkhard, M., 2004. Present-day geodynamics in the bend of the western and central Alps as constrained by earthqua.ke analysis. Geophys. J. Int. 158, 753–774. https://doi.org/10.1111/j.1365-246X.2004.02320.x.
Dercourt, J., Zonenshain, L.P., Ricou, L.E., Kazmin, V.G., Le Pichon, X., Knipper, A.L., Grandjacquet, C., Sbortshikov, I.M., Geyssant, J., Lepvrier, C., Pechersky, D.H., Boulin, J., Sibuet, J.C., Savostin, L.A., Sorokhtin, O., Westphal, M., Bazhenov, M.L., Lauer, J.P., Biju-Duval, B., 1986. Geological evolution of the Tethys belt from the Atlantic to the Pamirs since the Lias. Tectonophysics 123, 241–315.
Deschamps, A., Courboulex, F., Gaffet, S., Lomax, A., Virieux, J., Amato, A., Azzara, R., Castello, B., Chiarabba, C., Cimini, G.B., Cocco, M., Di Bona, M., Margheriti, L., Mele, F., Selvaggi, G., Chiaraluce, L., Piccinini, D., Ripepe, M., 2000. Spatio-temporal distribution of seismic activity during the Umbria-Marche crisis, 1997. J. Seismol. 4, 377–386. https://doi.org/10.1023/A:1026568419411.
Dewey, J.F., Helman, M.L., Turco, E., Hutton, D.H.W., Knott, S.D., 1989. Kinematics of the western Mediterranean. In: Coward, M.P., Dietrich, D. (eds.), Alpine Tectonic. Geol. Soc. Spec. Publicat. London 45, 265–283.
Di Domenica, A., Pizzi, A., 2017. Defining a mid-Holocene earthquake through speleoseismological and independent data: implications for the outer Central Apennines (Italy) seismotectonic framework. Solid Earth 8 (1), 161–176. https://doi.org/10.5194/se-8-161-2017.
Di Domenica, A., Petricca, P., Trippetta, F., Carminati, E., Calamita, F., 2014. Investigating fault reactivation during multiple tectonic inversions through mechanical and numerical modeling: an application to the Central-Northern Apennines of Italy. J. Struct. Geol. 67, 167–185.
Di Luccio, F., Ventura, G., Di Giovambattista, R., Piscini, A., Cinti, F.R., 2010. Normal faults and thrusts reactivated by deep fluids: the 6 April 2009 MW 6.3 L'Aquila earthquake, central Italy. J. Geophys. Res. 115, B06315. https://doi.org/10.1029/2009JB007190.
Di Luzio, E., Mele, G., Tiberti, M.M., Cavinato, G.P., Parotto, M., 2009. Moho deepening and shallow upper crustal delamination beneath the central Apennines. Earth Planet. Sci. Lett. 280 (1–4), 1–12. ISSN 0012-821X,. https://doi.org/10.1016/j.epsl.2008.09.018.
Di Stefano, R., Ciaccio, M.G., 2014. The lithosphere and asthenosphere system in Italy as inferred from the Vp and Vs 3D velocity model and Moho map. J. Geodyn. 82, 16–25. https://doi.org/10.1016/j.jog.2014.09.006.
Di Stefano, R., Chiarabba, C., Lucente, F., Amato, A., 1999. Crustal and uppermost mantle structure in Italy from the inversion of P-wave arrival times: geodynamic implications. Geophys. J. Int. 139, 483–498. https://doi.org/10.1046/j.1365-246x.1999.00952.x.
Di Stefano, R., Kissling, E., Chiarabba, C., Amato, A., Giardini, D., 2009. Shallow subduction beneath Italy: three-dimensional images of the Adriatic–European–Tyrrhenian litho-sphere system based on high-quality P wave arrival times. J. Geophys. Res. 114, B05305. https://doi.org/10.1029/2008JB005641.
Di Maro, R., Arcoraci, L., Battelli, P., Berardi, M., Castellano, C., Castello, B., Latorre, D., Marchetti, A., Margheriti, L., Mele, F., Nardi, A., Rossi, A., 2022. Bollettino Sismico Italiano 2015. Quad. Geofis. 176, 1–52. https://doi.org/10.13127/qdg/176.
Di Stefano, R., Bianchi, I., Ciaccio, M.G., Carrara, G., Kissling, E., 2011. Three-dimensional Moho topography in Italy: New constraints from receiver functions and controlled source seismology. Geochem. Geophys. Geosyst. 12, Q09006. https://doi.org/10.1029/2011GC003649.
DISS Working Group, . Database of Individual Seismogenic Sources (DISS), Version 3.2.1: A Compilation of Potential Sources for Earthquakes Larger than M 5.5 in Italy and Surrounding Areas. http://diss.rm.ingv.it/diss/. Istituto Nazionale di Geofisica e Vulcanologia. https://doi.org/10.6092/INGV.IT-DISS3.2.1.
Doglioni, C., Harabaglia, P., Merlini, S., Mongelli, F., Peccerillo, A., Piromallo, C., 1999. Orogens and slabs vs. their direction of subduction. Earth-Sci. Rev. 45, 167–208. https://doi.org/10.1016/S0012-8252(98)00045-2.
Efron, B., 1979. Bootstrap methods: another look at the Jackknife. Ann. Stat. 7 (1), 1–26. https://doi.org/10.1214/aos/ 1176344522.
Eva, E., Malusà, M.G., Solarino, S., 2015. A seismotectonic picture of the inner southern Western Alps based on the analysis of anomalously deep earthquakes. Tectonophysics 661, 190–199. https://doi.org/10.1016/j.tecto.2015.08.040.
Eva, E., Malusà, M.G., Solarino, S., 2020. Seismotectonics at the transition between opposite-dipping slabs (western Alpine region). Tectonics 39. https://doi.org/10.1029/2020TC006086 e2020TC006086.
Faccenna, C., Piromallo, C., Crespo-Blanc, L., Jolivet, L., Rossetti, F., 2004. Lateral slab deformation and the origin of Western Mediterranean arcs. Tectonics 23, TC1012. https://doi.org/10.1029/2002TC001488.
Faccenna, C., Becker, T.W., Auer, L., Billi, A., Boschi, L., Brun, J.P., Capitanio, F.A., Funiciello, F., Horvàth, F., Jolivet, L., Piromallo, C., Royden, L., Rossetti, F., Serpelloni, E., 2014. Mantle dynamics in the Mediterranean. Rev. Geophys. 52, 283–332. https://doi.org/10.1002/2013RG000444.
Fracassi, U., Burrato, P., Basili, R., Bencini, R., Di Bucci, D., Valensise, G., 2004. Shallow NE-SW extension and deep E-W right-lateral slip: coexisting seismogenic mechanisms as an expression of southern Italy geodynamics. In: Proceedings of the Gruppo Nazionale Geofisica Terra Solida Symposium, 23rd, Rome, December 2004 (Rome: Consiglio Nazionale delle Ricerche), pp. 200–202.
Frepoli, A., Maggi, C., Cimini, G.B., Marchetti, A., Chiappini, M., 2011. Seismotectonic of Southern Apennines from recent passive seismic experiments. J. Geodyn. 51 (2–3), 110–124.
Galadini, F., Galli, P., 2000. Active Tectonics in the Central Apennines (Italy) – Input Data for Seismic Hazard Assessment. Nat. Hazards 22, 225–268. https://doi.org/10.1023/A:1008149531980.
Galli, P., Giaccio, B., Peronace, E., Messina, P., 2015. Holocene paleoearthquakes and early–late pleistocene slip rate on the sulmona fault (Central Apennines, Italy). Bull. Seismol. Soc. Am. 105, 1–13. https://doi.org/10.1785/0120140029.
Ghisetti, F., Vezzani, L., 2002a. Normal faulting, extension and uplift in the outer thrust belt of the central Apennines (Italy): role of the Caramanico fault. Basin Res. 14, 225–236. https://doi.org/10.1046/j.1365-2117.2002.00171.x.
Ghisetti, F., Vezzani, L., 2002b. Normal faulting, transcrustal permeability and seismogenesis in the Apennines (Italy). Tectonophysics 348, 155–168.
Gori, S., Giaccio, B., Galadini, F., Falcucci, E., Messina, P., Sposato, A., Dramis, F., 2011. Active normal faulting along the Mt. Morrone south-western slopes (central Apennines, Italy). Int J Earth Sci (Geol Rundsch) 100, 157–171. https://doi.org/10.1007/s00531-009-0505-6.
Govoni, A., et al., 2014. The 2012 Emilia seismic sequence (Northern Italy): Imaging the thrust fault system by accurate aftershock location. Tectonophysics 622, 44–55. https://doi.org/10.1016/j.tecto.2014.02.013.
Grad, M., Brückl, E., Majdański, M., Behm, M., Guterch, A., CELEBRATION 2000, ALP 2002 Working Groups, 2009. Crustal structure of the Eastern Alps and their foreland: Seismic model beneath the CEL10/Alp04 profile and tectonic implications. Geophys. J. Int. 177, 279–295. https://doi.org/10.1111/j.1365-246X.2008.04074.x.
Grenerczy, G., Sella, G., Stein, S., Kenyeres, A., 2005. Tectonic implications of the GPS velocity field in the northern Adriatic region. Geophys. Res. Lett. 32, L16311. https://doi.org/10.1029/2005GL022947.
Gualandi, A., Nichele, C., Serpelloni, E., Chiaraluce, L., Anderlini, L., Latorre, D., Belardinelli, M.E., Avouac, J.-P., 2017. Aseismic deformation associated with an earthquake swarm in the northern Apennines (Italy). Geophys. Res. Lett. 44, 7706–7714. https://doi.org/10.1002/2017GL073687.
Gvirtzman, Z., Nur, A., 1999. The formation of Mount Etna as the consequence of slab rollback. Nature 401, 782–785. https://doi.org/10.1038/44555.
Haessler, H., Gaulon, R., Rivera, L., Console, R., Frogneux, M., Gasparini, G., Martel, L., Patau, G., Siciliano, M., Cisternas, A., 1988. The Perugia (Italy) earthquake of 29 April 1984: a micro- earthquake survey. Bull. Seismol. Soc. Am. 78, 1948–1964.
Handy, M.R., Schmid, S.M., Bousquet, R., Kissling, E., Bernoulli, D., 2010. Reconciling plate-tectonic reconstructions of Alpine Tethys with the geological–geophysical

record of spreading and subduction in the Alps. Earth-Sci. Rev. 102, 121–158. https://doi.org/10.1016/j.earscirev.2010.06.002.
Hunstad, I., Selvaggi, G., D'Agostino, N., England, P., Clarke, P., Pierozzi, M., 2003. Geodetic strain in peninsular Italy between 1875 and 2001. Geophys. Res. Lett. 30, 1181. https://doi.org/10.1029/2002GL016447.
Husen, S., Smith, R.B., 2004. Probabilistic earthquake relocation in three-dimensional velocity models for the Yellowstone National Park Region. Wyoming. Bull. Seismol. Soc. Am. 94, 880–896. https://doi.org/10.1785/0120030170.
Husen, S., Kissling, E., Deichmann, N., Wiemer, S., Giardini, D., Baer, M., 2003. Probabilistic earthquake location in complex three-dimensional velocity models: Application to Switzerland. J. Geophys. Res. 108, 2077. https://doi.org/10.1029/2002JB001778.
Improta, L., Latorre, D., Margheriti, L., Nardi, A., Marchetti, A., Lombardi, A.M., Castello, B., Villani, F., Ciaccio, M.G., Mele, F.M., Moretti, M., The Bollettino Sismico Italiano Working Group, 2019. Multi-segment rupture of the 2016 Amatrice-Visso-Norcia seismic sequence (central Italy) constrained by the first high-quality catalog of Early Aftershocks. Sci. Report. 9, 6921. https://doi.org/10.1038/s41598-019-43393-2.
ISIDe Working Group, 2007. Italian Seismological Instrumental and Parametric Database (ISIDe). Istituto Nazionale di Geofisica e Vulcanologia (INGV). https://doi.org/10.13127/ISIDE.
Latorre, D., Amato, A., Chiarabba, C., 2010. High-resolution seismic imaging of the Mw5.7, 2002 Molise, southern Italy, earthquake area: evidence of deep fault reactivation. Tectonics 29, TC4014. https://doi.org/10.1029/2009TC00 2595.
Latorre, D., Mirabella, F., Chiaraluce, L., Trippetta, F., Lomax, A., 2016. Assessment of earthquake locations in 3-D deterministic velocity models: a case study from the altotiberina near fault observatory (Italy). J. Geophys. Res. Solid Earth 121, 8113–8135. https://doi.org/10.1002/2016JB013170.
Lavecchia, G., Brozzetti, F., Barchi, M., Menichetti, M., Keller, J.V., 1994. Seismotectonic zoning in east-central Italy deduced from an analysis of the Neogene to present deformations and related stress fields. Geol. Soc. Am. Bull. 106, 1107–1120. https://doi.org/10.1130/0016-7606(1994)106<1107:SZIECI>2.3.CO;2.
Livani, M., Scrocca, D., Arecco, P., Doglioni, C., 2018. Structural and stratigraphic control on salient and recess development along a thrust belt front: the Northern Apennines (Po Plain, Italy). J. Geophys. Res. Solid Earth 123. https://doi.org/10.1002/2017JB015235.
Lomax, A., 2005. A reanalysis of the hypocentral location and related observations for the great 1906 California earthquake. Bull. Seismol. Soc. Am. 95, 861–877. https://doi.org/10.1785/0120040141.
Lomax, A., 2008. Location of the focus and tectonics of the focal region of the California earthquake of 18 April 1906. Bull. Seismol. Soc. Am. 98, 846–860. https://doi.org/10.1785/0120060405.
Lomax, A., 2020. Absolute location of 2019 ridgecrest seismicity reveals a shallow M w 7.1 hypocenter, migrating and Pulsing Mw 7.1 Foreshocks, and Duplex M w 6.4 Ruptures. Bull. Seismol. Soc. Am. 110, 1845–1858. https://doi.org/10.1785/0120200006.
Lomax, A., Curtis, A., 2001. Fast, probabilistic earthquake location in 3D models using oct-tree importance sampling. Geophys. Res. Abstr. 3, 955.
Lomax, A., Virieux, J., Volant, P., Berge-Thierry, C., 2000. Probabilistic earthquake location in 3D and layered models. In: Thurber, C.H., Rabinowitz, N. (Eds.), Advances in Seismic Event Location. Modern Approaches in Geophysics, vol. 18. Springer, Dordrecht, The Netherlands, pp. 101–134. https://doi.org/10.1007/978-94-015-9536-0_5.
Lomax, A., Michelini, A., Curtis, A., 2014. Earthquake location, direct, global-search methods. In: Meyers, R.A. (Ed.), Encyclopedia of Complexity and System Science, Second Ed. Springer, New York, New York, pp. 1–33. https://doi.org/10.1007/978-3-642-27737-5_150-2.
Lucente, F.P., Chiarabba, C., Cimini, G.B., Giardini, D., 1999. Tomographic constraints on the geodynamic evolution of the Italian region. J. Geophys. Res. 104, 20307–20327. https://doi.org/10.1029/1999JB900147.
Magnoni, F., Casarotti, E., Di Komatitsch, D., Stefano, R., Ciaccio, M.G., Melini, D., Michelini, A., Piersanti, A., 2022. Adjoint tomography of the Italian lithosphere. Commun Earth Environ 3, 69. https://doi.org/10.1038/s43247-022-00397-7.
Malusà, M.G., Zhao, L., Eva, E., Solarino, S., Paul, A., Guillot, S., Schwartz, S., Dumont, T., Aubert, C., Salimbeni, S., Pondrelli, S., Wang, Q., Zhu, R., 2017. Earthquakes in the western Alpine mantle wedge. Gondwana Res. 44, 89–95. https://doi.org/10.1016/j.gr.2016.11.012.
Mantovani, E., Albarello, D., Tamburelli, C., Babbucci, D., Viti, M., 1997. Plate convergence, crustal delamination, extrusion tectonics and minimization of shortening work as main controlling factors of the recent Mediterranean deformation pattern. Ann. Geophys. [Internet]. https://doi.org/10.4401/ag-3894. Nov. 25.
Marchetti, A., Ciaccio, M.G., Nardi, A., Bono, A., Mele, F.M., Margheriti, L., Rossi, A., Battelli, P., Melorio, C., Castello, B., Lauciani, V., Berardi, M., Castellano, C., Arcoraci, L., Lozzi, G., Battelli, A., Thermes, C., Pagliuca, N., Modica, G., Lisi, A., Pizzino, L., Baccheschi, P., Pintore, S., Quintiliani, M., Mandiello, A., Marcocci, C., Fares, M., Cheloni, D., Frepoli, A., Latorre, D., Lombardi, A.M., Moretti, M., Pastori, M., Vallocchia, M., Govoni, A., Scognamiglio, L., Basili, A., Michelini, A., Mazza, S., 2016. The Italian Seismic Bulletin: strategies, revised pickings and locations of the Central Italy seismic sequence. Ann. Geophys. 59. https://www.annalsofgeophysics.eu/index.php/annals/article/view/7169.
Margheriti, L., Nostro, C., Cocina, O., Castellano, M., Moretti, M., Lauciani, V., Quintiliani, M., Bono, A., Mele, F.M., Pintore, S., et al., 2021. Seismic surveillance and earthquake monitoring in Italy. Seismol. Res. Lett. XX 1–13. https://doi.org/10.1785/0220200380.
Martinis, B., Pieri, M., 1964. Alcune notizie sulla formazione evaporitica del Triassico Superiore nell'Italia centrale e meridionale. Mem. Soc. Geol. Ital. 4, 649–678.
Marzorati, M., Massa, M., Cattaneo, M., Monachesi, G., Frapiccini, M., 2014. Very detailed seismic pattern and migration inferred from the April 2010 Pietralunga (northern Italian Apennines) micro-earthquake sequence. Tectonophysics 610, 91–109. https://doi.org/10.1016/j.tecto.2013.10.014.
Mazza, S., Morelli, A., Boschi, E., 1998. Near real-time data collection and processing at MEDNET. In: EOS Trans. AGU79, F569.
Mele, G., Sandvol, E., 2003. Deep crustal roots beneath the northern Apennines inferred from teleseismic receiver functions. Earth Planet. Sci. Lett. 211, 69–78. https://doi.org/10.1016/S0012-821X(03)00185-7.
Michele, M., Di Stefano, R., Chiaraluce, L., Cattaneo, M., De Gori, P., Monachesi, G., Latorre, D., Marzorati, S., Valoroso, L., Ladina, C., Chiarabba, C., Lauciani, V., Fares, M., 2016. The Amatrice 2016 seismic sequence: a preliminary look at the mainshock and aftershocks distribution. Ann. Geophys. 59 https://doi.org/10.4401/ag-7227.
Michele, M., Latorre, D., Emolo, A., 2019. An Empirical Formula to Classify the Quality of Earthquake Locations. Bull. Seismol. Soc. Am. 109, 2755–2761. https://doi.org/10.1785/0120190144.
Michele, M., Chiaraluce, L., Di Stefano, R., Waldhauser, F., 2020. Fine-scale structure of the 2016–2017 Central Italy seismic sequence from data recorded at the Italian National Network. J. Geophys. Res. 125 https://doi.org/10.1029/2019JB018440 e2019JB018440.
Molli, G., Crispini, L., Malusà, M.G., Mosca, P., Piana, F., Federico, L., 2010. Geology of the Western Alps-Northern Apennine junction area: a regional review. J. Virtual Explor. 36 https://doi.org/10.3809/jvirtex.2009.00215.
Mongelli, F., Zito, G., 2000. The thermal field in a basin after a sudden passive pure shear lithospheric extension and sublithospheric mechanical erosion: the case of the Tuscan Basin (Italy). Geophys. J. Int. 142, 142–150. https://doi.org/10.1046/j.1365-246x.2000.00142.x.
Montone, P., Mariucci, M.T., 2016. The new release of the Italian contemporary stress map. Geophys. J. Int. 205, 1525–1531. https://doi.org/10.1093/gji/ggw100.
Montuori, C., Cimini, G.B., Favali, P., 2007. Teleseismic tomography of the southern Tyrrhenian subduction zone: New results from seafloor and land recordings. J. Geophys. Res. 112, B03311. https://doi.org/10.1029/2005JB004114.
Nardi, A., Arcoraci, L., Battelli, P., Berardi, M., Castellano, C., Marchetti, A., Margheriti, L., Mele, F., Rossi, A., 2020. Bollettino Sismico Italiano 2014. Quad. Geofis. 165, 1–48. https://doi.org/10.13127/qdg/165.
Nostro, C., Cocco, M., Belardinelli, M.E., 1997. Static stress change in extensional regimes: an application to southern Apennines (Italy). J. Geophys. Res. 87, 234–248.
Pantosti, D., Valensise, G., 1990. Faulting mechanism and complexity of the November 23, 1980, Campania-Lucania Earthquake, inferred from surface observations. J. Geophys. Res. 95, 15319–15341.
Patacca, E., Scandone, P., 2001. Late thrust propaga- tion and sedimentary response in the thrust-belt-fore- deep system of the Southern Apennines (Pliocene- Pleistocene). In: Vai, G.B., Martini, P. (Eds.), Anatomy of an Orogene: The Apennines and Adjacent Mediterranean Basin. Kluwer Academic Publishers, pp. 401–440.
Pialli, G., Barchi, M., Minelli, G., 1998. In: Pialli, G., Barchi, M., Minelli, G. (Eds.), Results of the CROP03 deep seismic reflection profile : atti del convegno "Presentazione dei risultati del profilo sismico CROP03" Roma, 7-9 novembre 1996.
Piana Agostinetti, N., Lucente, F.P., Selvaggi, G., Di Bona, M., 2002. Crustal Structure and Moho Geometry beneath the Northern Apennines (Italy). Geophys. Res. Lett. 29, 2002. https://doi.org/10.1029/2002GL015109.
Pieri, P., Sabato, L., Loiacono, F., Marino, M., 1994. Il bacino di piggyback di Sant'Arcangelo: evoluzione tettonico-sedimentaria. Mem. Soc. Geol. It. 113, 465–481.
Pieri, P., Vitale, G., Beneduce, P., Doglioni, C., Gallicchio, S., Giano, S.I., Loizzo, R., Moretti, M., Prosser, G., Sabato, L., Schiattarella, M., Tramutoli, M., Tropeano, M., 1997. Tettonica quaternaria nell'area bradanico-ionica, Il Quaternario. Italian J. Quatern. Sci. 10 (2), 535–542.
Pizzi, A., Galadini, F., 2009. Pre-existing cross-structures and active fault segmentation in the northern-central Apennines (Italy). Tectonophysics 476, 304–319. https://doi.org/10.1016/j.tecto.2009.03.018.
Podvin, P., Lecomte, I., 1991. Finite difference computation of traveltimes in very contrasted velocity models: a massively parallel approach and its associated tools. Geophys. J. Int. 105, 271–284. https://doi.org/10.1111/j.1365-246X.1991.tb03461.x.
Polonia, A., Torelli, L., Mussoni, P., Gasperini, L., Artoni, A., Klaeschen, D., 2011. The Calabrian Arc subduction complex in the Ionian Sea: Regional architecture, active deformation, and seismic hazard. Tectonics 30, TC5018. https://doi.org/10.1029/2010TC002821.
Polonia, A., Torelli, L., Artoni, A., Carlini, M., Faccenna, C., Ferranti, L., Gasperini, L., Govers, R., Klaeschen, D., Monaco, C., Neri, G., Nijholt, N., Orecchio, B., Wortel, R., 2016. The Ionian and Alfeo–Etna fault zones: New segments of an evolving plate boundary in the central Mediterranean Sea? Tectonophysics 675, 69–90. https://doi.org/10.1016/j.tecto.2016.03.016.
Pondrelli, S., Salimbeni, S., Ekström, G., Morelli, A., Gasperini, P., Vannucci, G., 2006. The Italian CMT dataset from 1977 to the present. Phys. Earth Planet. Inter. 159, 286–303. https://doi.org/10.1016/j.pepi.2006.07.008.
Rovida, A., Locati, M., Camassi, R., Lolli, B., Gasperini, P., 2020. The Italian earthquake catalogue CPTI15. Bull. Earthq. Eng. 18, 2953–2984. https://doi.org/10.1007/s10518-020-00818-y.
Rovida, A., Locati, M., Camassi, R., Lolli, B., Gasperini, P., Antonucci, A., 2022. Catalogo Parametrico dei Terremoti Italiani (CPTI15), versione 4.0. Istituto Nazionale di Geofisica e Vulcanologia (INGV). https://doi.org/10.13127/CPTI/CPTI15.4.
Scarfì, L., Barberi, G., Barreca, G., Cannavò, F., Koulakov, I., Patanè, D., 2018. Slab narrowing in the Central Mediterranean: the Calabro-Ionian subduction zone as

imaged by high resolution seismic tomography. Sci. Rep. 8, 5178. https://doi.org/10.1038/s41598-018-23543-8.
Schmid, S.M., Kissling, E., Diehl, T., van Hinsbergen, D.J.J., Molli, G., 2017. Ivrea mantle wedge, arc of the Western Alps, and kinematic evolution of the Alps–Apennines orogenic system. Swiss J. Geosci. 110, 581–612. https://doi.org/10.1007/s00015-016-0237-0.
Scholz, C., 2019. The Mechanics of Earthquakes and Faulting. Cambridge University Press, Cambridge. https://doi.org/10.1017/9781316681473.
Schorlemmer, D., Mele, F., Marzocchi, W., 2010. A completeness analysis of the National Seismic Network of Italy. J. Geophys. Res. 115, B04308. https://doi.org/10.1029/2008JB006097.
Scognamiglio, L., Margheriti, L., Mele, F.M., Tinti, E., Bono, A., et al., 2012. The 2012 Pianura Padana Emiliana seismic sequence: locations, moment tensors and magnitudes. Ann. Geophys. 55, 549–559. https://doi.org/10.4401/ag-6159.
Selvaggi, G., Castello, B., Azzara, R., 1997. Spatial distribution of scalar seismic moment release in Italy (1983-1996): seismotectonic implications for the Apennines. Ann. Geophys. 40 (6) https://doi.org/10.4401/ag-3832.
Serri, G., Innocenti, F., Manetti, P., 1993. Geochemical and petrological evidence of the subduction of delaminated Adriatic continental litho-sphere in the genesis of the Neogene-Quaternary magmatism of Central Italy. Tectonophysics 223, 117–147. https://doi.org/10.1016/0040-1951(93)90161-C.
Sgroi, T., Polonia, A., Barberi, G., Billi, A., Gasperini, L., 2021. New seismological data from the Calabrian arc reveal arc-orthogonal extension across the subduction zone. Sci. Report. 11, 473. https://doi.org/10.1038/s41598-020-79719-8.
Slejko, D., Neri, G., Orozova, I., Renner, G., Wyss, M., 1999. Stress Field in Friuli (NE Italy) from fault plane solutions of activity following the 1976 main shock. Bull. Seismol. Soc. Am. 89, 1037–1052. https://doi.org/10.1785/BSSA0890041037.
Stampfli, G.M., Borel, G.D., 2002. A plate tectonic model for the paleozoic and mesozoic constrained by dynamic plate boundaries and restored synthetic oceanic isochrons. Earth Planet. Sci. Lett. 196, 17–33. https://doi.org/10.1016/S0012-821X(01)00588-X.
Sue, C., Thouvenot, F., Frechet, J., Tricart, P., 1999. Widespread extension in the core of the western Alps revealed by earthquake analysis. J. Geophys. Res. 104, 25611–25622. https://doi.org/10.1029/1999JB900249.
Tarantola, A., Valette, B., 1982. Inverse problems = quest for information. J. Geophys. 50, 159–170.
Tavarnelli, E., Butler, R.W.H., Decandia, F.A., Calamita, F., Grasso, M., Alvarez, W., Renda, P., 2004. Implications of fault reactivation and structural inheritance in the Cenozoic tectonic evolution of Italy. In: Crescenti, U., D'Offizi, S., Merlini, S., Sacchi, R. (Eds.), Geology of Italy - Special Volume of the Sociatà Geologica Italiana for the 32nd International Geological Congress (IGC 32), Florence, vol. 2004, pp. 209–222.
Thouvenot, F., Frechet, J., 2005. In: Pinter, N., et al. (Eds.), Seismicity at the North-Western Edge of Adria, NATO Science Series, vol. 4. Springer, New York, pp. 335–350.
Trionfera, B., Frepoli, A., De Luca, G., De Gori, P., Doglioni, C., 2020. The 2013–2018 matese and beneventano seismic sequences (Central– Southern Apennines): new constraints on the hypocentral depth determination. Geosciences 10, 17. https://doi.org/10.3390/geosciences10010017.
Trippetta, F., Collettini, C., Vinciguerra, S., Meredith, P.G., 2010. Laboratory measurements of the physical properties of Triassic Evaporites from Central Italy and correlation with geophysical data. Tectonophysics 492, 121–132. https://doi.org/10.1016/j.tecto.2010.06.001.
Valensise, G., Pantosti, D., Basili, R., 2004. Seismology and tectonic setting of the 2002 Molise, Italy. Earthquake. Earthquake Spectra. 20 (Suppl. 1), 23–37. https://doi.org/10.1193/1.1756136.
Valoroso, L., Improta, L., Chiaraluce, L., Di Stefano, R., Ferranti, L., Govoni, A., Chiarabba, C., 2009. Active faults and induced seismicity in the Val d'Agri area (Southern Apennines, Italy). Geophys. J. Int. 178, 488–502. https://doi.org/10.1111/j.1365-246X.2009.04166.x.
Vuan, A., Sugan, M., Chiaraluce, L., Di Stefano, R., 2017. Loading rate variations along a midcrustal shear zone preceding the MW 6.0 earthquake of 24 August 2016 in Central Italy. Geophys. Res. Lett. 44, 12–70.
Waldhauser, F., Michele, M., Chiaraluce, L., Di Stefano, R., Schaff, D.P., 2021. Fault planes, fault zone structure and detachment fragmentation resolved with high-precision aftershock locations of the 2016–2017 Central Italy sequence. Geophys. Res. Lett. 48 (16) e2021GL092918.
Watts, A.B., Burov, E.B., 2003. Lithospheric strength and its relationship to the elastic and seismogenic layer thickness. Earth Planet. Sci. Lett. 213, 113–131. https://doi.org/10.1016/S0012-821X(03)00289-9.
Wessel, P., Luis, J.F., Uieda, L., Scharroo, R., Wobbe, F., Smith, W.H.F., Tian, D., 2019. The Generic Mapping Tools version 6. Geochem. Geophys. Geosyst. 20, 5556–5564.
Westway, R., Jackson, J., 1987. The earthquake of the 1980 November 23 in Campania-Basilicata (southern Italy). Geophys. J. Int. 90, 375–443. https://doi.org/10.1111/j.1365-246X.1987.tb00733.x.
Wortel, M.J.R., Spakman, W., 1992. Structure and dynamics of subducted lithosphere in the Mediterranean region. Proc. Kon. Ned. Acad. Wetensch. 95, 325–347.
Wortel, M.J.R., Spakman, W., 2000. Subduction and slab detachment in the Mediterranean-Carpathian region. Science 290, 1910–1917.
Zhao, D., Hasegawa, A., Horiuchi, S., 1992. Tomographic imaging of P and S wave velocity structure beneath northeastern Japan. J. Geophys. Res. 97 (B13), 19909–19928.
Zhao, D., Hasegawa, A., Kanamori, H., 1994. Deep structure of Japan subduction zone as derived from local, regional, and teleseismic events. J. Geophys. Res. 99 (B11), 22313–22329.